NK cells shape the clonal evolution of B cell leukaemia by IFN-γ production

Michelle C. Buri[1], Mohamed R. Shoeb[1], Aleksandr Bykov[1], Peter Repiscak[1], Hayeon Baik[1], Alma Dupanovic[1], Faith O. David[1], Boris Kovacic[1], Faith Hall-Glenn[1], Jos Urbanus[2], Lisa Sippl[1], Susanne Stofner[1], Dominik Emminger[1,3], Jason Cosgrove[4], Manfred Lehner[1,3], Leïla Perié[4], Ton N. Schumacher[2,5], Dagmar Gotthardt[6], Florian Halbritter[1], Eva M. Putz[1,7,#]

[1] St. Anna Children's Cancer Research Institute (CCRI), Vienna, Austria

[2] Division of Molecular Oncology & Immunology, Oncode Institute, Netherlands Cancer Institute, Amsterdam, The Netherlands

[3] Christian Doppler Laboratory for Next Generation CAR T Cells, Vienna, Austria

[4] Institut Curie, Université PSL, Sorbonne Université, CNRS UMR168, Laboratoire Physico Chimie Curie, Paris, France

[5] Department of Hematology, Leiden University Medical Center, Leiden, The Netherlands.

[6] Institute of Pharmacology, University of Veterinary Medicine Vienna, Vienna, Austria

[7] Center for Physiology and Pharmacology, Institute of Pharmacology, Medical University of Vienna, Vienna, Austria

Correspondence to Eva M. Putz, Institute of Pharmacology, Medical University of Vienna, Waehringerstrasse 13A, 1090 Vienna, Austria, eva-maria.putz@meduniwien.ac.at

Word count: 199 (Abstract) and 4492 (Introduction, Results, Discussion)

Number of figures: 5

Number of supplementary figures: 7

Number of supplementary tables: 4

Keywords: cancer immunoediting, natural killer cells, tumour evolution, cytotoxicity, effector function, interferon-γ, perforin, Ly6A

Abstract

The term cancer immunoediting describes the dual role by which the immune system can suppress and promote tumour growth and is divided into three phases: elimination, equilibrium and escape. The role of NK cells has mainly been attributed to the elimination phase. Here we show that NK cells play a role in all three phases of cancer immunoediting. Extended co-culturing of DNA barcoded mouse BCR/ABL^{p185+} B acute lymphoblastic leukaemia cells with NK cells allowed for a quantitative measure of NK cell-mediated immunoediting. Whereas most tumour cell clones were efficiently eliminated by NK cells, a certain fraction of tumour cells harboured an intrinsic resistance. Furthermore, DNA barcoding revealed tumour cell clones with secondary resistance, which stochastically acquired resistance to NK cells. We found that the production of interferon-γ (IFN-γ) rather than direct cytotoxicity by NK cells, led to the emergence of highly resistant tumour cells. Besides well-known regulators of immune evasion, our analysis of NK resistant tumour cells revealed the upregulation of novel genes, such as *Ly6a*, which drives NK cell resistance in leukaemic cells. Our results demonstrate that tumour cells are actively edited by NK cells during the equilibrium phase and use different avenues to escape NK cell-mediated eradication.

39 # Main/Introduction

40 Cancer immunoediting refers to the dynamic interaction between immune cells and cancer cells during
41 tumour development[1]. The immune system can have both tumour-promoting and tumour-suppressive
42 effects. This process occurs in three phases: elimination, equilibrium, and escape. In the elimination
43 phase, adaptive and innate immune cells, particularly cytotoxic T and NK cells, recognise and eliminate
44 cancer cells. The equilibrium phase involves the coexistence of tumour cells and the immune system,
45 leading to sculpting of the tumour under constant immune pressure, ultimately resulting in immune
46 escape[2].

47 NK cells are innate lymphoid cells with the ability of recognising and eliminating damaged, stressed,
48 and infected cells including cancer cells[3]. NK cell activation relies on a balance of activating and
49 inhibitory signals from receptors on their surface during the interaction with potential target cells. On
50 the one hand, activated NK cells can kill target cells through exocytosis of cytotoxic granules containing
51 perforin and granzymes[4], induction of death receptor-mediated apoptosis[5] or antibody-dependent
52 cellular cytotoxicity (ADCC) via their FcγRIIIA (CD16) receptor[6]. On the other hand, NK cells secrete
53 cytokines such as interferon-γ (IFN-γ), which activate other immune cells in their vicinity[7,8]. In the
54 context of cancer immunoediting, NK cells play a crucial role in eliminating tumour cells during the
55 elimination phase and limiting the metastatic spread of tumour cells. NK cells spare healthy tissue and
56 present a safe treatment option with minimal risk of causing adverse effect such as cytokine release
57 syndrome or graft versus host disease[9]. As a result, there is growing interest in using NK cells for
58 immunotherapies, which will benefit from a better understanding of how tumour cells evade NK cell
59 attacks to effectively target their Achilles heel. However, most studies to date have focused on the
60 interaction between human NK cells and tumour cell lines obtained from patients[10–15]. These tumour
61 cells have already successfully evaded from the patient´s immune system and may thus not represent
62 suitable models to study immunoediting.

63 Here, we used a model based on non-edited NK cell-naïve mouse BCR/ABL^{p185+} B cell acute
64 lymphoblastic leukaemia (B-ALL) cells to investigate the primary interaction of tumour cells with NK

65 cells. This model involves a long-term co-culture of tumour cells and primary NK cells. By analysing the
66 NK cell-resistant tumour cells that emerge during the co-culture, we investigated molecular changes
67 using RNA sequencing (RNA-seq) and assay for transposase-accessible chromatin sequencing (ATAC-
68 seq). The results indicate that the transcriptomic changes in the resistant tumour cells are mainly due
69 to IFN-γ secretion by NK cells, which upregulates genes like lymphocyte antigen 6 complex, locus A
70 (*Ly6a*) and phospholipase A and acyltransferase 3 (*Plaat3*). This study identified Ly6A as novel potential
71 driver of NK cell-mediated immune evasion of leukaemia. Moreover, we established a model to
72 quantify NK cell effector functions and their ability to edit DNA barcoded tumour cells. Cellular DNA
73 barcoding stably introduces unique inheritable DNA sequences that allows tracking of individual cell
74 clones and their fates within a heterogeneous cell population[16–18]. Thereby, we observed that, while
75 some tumour cells were inherently resistant or sensitive to NK cells, a few tumour cells were edited by
76 NK cells to become resistant. In summary, this study shows that NK cells play an important role in all
77 three phases of cancer immunoediting and contribute to the active sculpting of tumour cell clones,
78 ultimately driving tumour evasion.
79

80 Results

81 Quantitative measure of NK effector functions

82 As a model to study NK cell evasion of leukaemic tumour cells we established a long-term *in vitro* co-
83 culture system using IL-2-activated primary mouse NK cells co-incubated with NK-naïve DNA barcoded
84 B-ALL cell lines for up to 20 days (**Figure 1A**). We generated several independent B-ALL cell lines from
85 the bone marrow of wild-type (n=10) and major histocompatibility complex 1 (MHC-1)-deficient *B2m*$^{-}$
86 $^{/-}$ mice (n=10) and characterised their NK receptor ligand surface expression and their susceptibility
87 towards NK cell-mediated eradication at an effector-to-target (E:T) ratio of 10:1. Summarizing this data
88 by unsupervised hierarchical clustering (**Figure 1B**) highlighted the two wild-type cell lines #13 and #15
89 which showed the highest susceptibility towards NK cells and expressed enhanced levels of activating

90 NKG2D-ligand Rae1 and lower levels of inhibitory ligands (e.g. classical and non-classical MHC-1
91 proteins H2-K^b, H2-D^b, Qa-1^b and Qa-2). *B2m*-deficient B-ALL cell lines showed a higher susceptibility
92 towards NK cells according to the recognition of missing self[19] (see **Figure S1A** for full characterisation).
93 To allow for a systematic quantification of NK cell effector functions, a DNA barcode library was
94 introduced into the wild-type B-ALL cell lines #13 and #15 (n=2 each) and the *B2m*$^{-/-}$ (n=1) cell line #23
95 to track individual tumour cell clones over time. For this purpose, a new lentiviral barcode library
96 (LG2.1, containing 52,645 barcodes in the reference list) was generated consisting of 21 random
97 nucleotides positioned downstream of a green fluorescent protein (*GFP*) gene (**Figures S1B-E**). The
98 lentiviral library was introduced into the B-ALL cell lines at a low multiplicity of infection (MOI) to
99 ensure the integration of a single barcode per cell as previously described[20,21] (**Figure 1C**). To enrich for
100 barcoded cells, GFP$^+$ cells were FACS sorted shortly after transduction and before the long-term co-
101 culture with IL-2-activated NK cells. The barcode diversity of the resulting four cell lines called A and B
102 (derived from #13), C and D (derived from #15) was determined by site-specific PCR amplification and
103 next generation sequencing (**Figure 1D**). The barcoded cells were co-incubated with IL-2-activated NK
104 cells at an E:T ratio of 1:1. After 4 and 14 days, GFP$^+$ tumour cells were FACS purified and fresh NK cells
105 were replenished to re-challenge the tumour cells. Throughout the experiment, the absolute number
106 of GFP$^+$ tumour cells was determined by regular flow cytometric analysis (**Figure 1E**). While the tumour
107 cells initially showed significantly slower proliferation in the presence of NK cells during the first two
108 rounds of co-culture, this difference became marginal in the third round. Twenty-nine days after the
109 start of co-culture, we performed a classical 4-hour cytotoxicity assay with tumour cells that had been
110 co-cultured with NK cells for 20 days versus NK-naïve tumour cells. As shown in **Figure 1F**, extended
111 co-culture of NK and leukaemic cells induced resistance towards NK cell-mediated killing and led to
112 tumour evasion *in vitro*.

113 NK cell-mediated editing of leukaemic cells

114 There are four conceivable fates of B-ALL tumour cell clones upon long-term co-culture with NK cells:
115 The abundance of one clone could be lower ("eliminated"), higher ("primary resistant"), unchanged

116 (“static”) or highly variable (“secondary resistant”) (**Figure 2A**). After bulk DNA sequencing of the
117 barcodes, we designed a decision tree to discriminate these four categories algorithmically (**Figure 2B**).
118 Primary resistance, also known as intrinsic resistance[22], is defined as *a priori* resistance towards
119 therapy. In our study, primary resistance was characterised by a reproducible and significant
120 accumulation despite the presence of NK cells in co-culture. In comparison, secondary resistance
121 describes the phenomenon of acquired resistance, represented by a situation in which a tumour can
122 initially respond effectively to therapy but relapse or progress after treatment[23]. We hypothesised that
123 acquired secondary resistance was not a tumour-intrinsic property but acquired only in a subfraction
124 of sibling cells and would be observed in isolated wells (**Figure 2A**). Indeed, clustering the DNA
125 barcoded leukaemic cells according to our four pre-defined categories (**Figure 2C, S2A** for summary
126 data), showed that the majority of leukaemic cell clones was efficiently eliminated (58.5±1.4%
127 considering n=2-3 independent experiments comprising n=2-4 B-ALL cell lines, mean±SEM). Only a
128 smaller number of leukaemic cell clones seemed to have an NK cell resistant phenotype (14.3±1.3%).
129 About 23.9±1.4% of the B-ALL cell clones remained static despite the presence of NK cells. As
130 hypothesised, we also observed B-ALL cell clones that showed secondary resistance, characterised by
131 the presence of the cell clone in only 1/3 replicate wells (3.3±0.8%, **Figure 2D**). To be able to draw
132 conclusions about the pre-existing fate of the tumour cell clones, we compared two independent
133 experiments with the same barcoded cell lines. As shown in **Figures 2E and S2B**, the cell clones
134 attributed to the clusters primary resistant and eliminated were found to have the same fate in both
135 experiments. In contrast, the pool of secondary resistant tumour cell clones was distinctive for
136 independent experiments. In summary, our data suggest that, whereas primary resistant and
137 eliminated cells harbour tumour-intrinsic properties *a priori* that determine their destiny, the fate of
138 secondary resistant tumour cell clones is stochastic. This underscores our hypothesis that secondary
139 resistant tumour cells acquire their resistant phenotype during NK co-culture. Our data clearly show
140 that apart from direct killing, NK cells participate in immunoediting by actively shaping the
141 tumourigenicity of individual tumour cells.

142 ## Molecular changes observed in NK cell resistant B-ALL cells

143 To identify novel drivers of NK cell resistance we investigated the changes in the transcriptomic and
144 chromatin accessibility profiles of the NK cell-resistant B-ALL cell lines generated during the long term
145 *in vitro* co-culture. To this end, we performed RNA (**Figures 3A-D, S3A-E**) and ATAC sequencing (**Figures**
146 **3E-F, S4A-C**) and compared NK co-cultured to NK naïve tumour cells. The transcriptomic analysis
147 showed a significant upregulation of genes with a well-known link to NK cell immune evasion such as
148 several components of the MHC-I machinery (e.g., *Stat1*, *B2m*, *Tap1* and *H2-K1*[24]) (**Figure 3A, Figures**
149 **S3C-F**). Additionally, this analysis revealed a novel set of genes, which may include potential drivers of
150 NK cell resistance, such as *Ly6a* and *Plaat3*. The functional enrichment analysis showed that the main
151 biological process associated with the differentially expressed genes was the response to IFN-γ (e.g.,
152 *Stat1*, *Irf1*, *Ccl5* and *Cd74*) (**Figure 3B**), which is produced by activated NK cells in co-culture. After
153 integrating the results from the four barcoded cell lines A-D, we observed that many differentially
154 expressed genes upon NK cell co-culture were cell line specific (up: A/B=193 and C/D=99, down: A/B:
155 211 and C/D=63). However, a total of 129 genes were up- and 27 were downregulated in all four cell
156 lines and may be universally associated with or driving NK cell escape (**Figure 3C**). The top-30
157 differentially regulated genes are depicted in the heat map in **Figure 3D**. In line, the ATAC sequencing
158 results showed the opening of chromatin at the promoters of classical interferon-inducible genes (e.g.,
159 *Iigp1*, *Ifi27*, *Mx1*), as well as *Ly6a* and *Plaat3*, genes previously observed in the RNA sequencing dataset
160 (**Figure 3E, S4C**). We considered overlapping differentially accessible regions (DARs) in cell lines A/B
161 and C/D as the most robust ones (**Figure 3F**). Integration of RNA and ATAC sequencing data by
162 comparing the differentially expressed genes and accessible regions in cell lines A/B showed a
163 significant intersection (37 genes up/open, 16 genes down/closed). Interestingly, the two highly
164 upregulated genes *Ly6a* and *Plaat3* in the transcriptomic analysis were also present in this strictly
165 filtered data set (**Figure 3G**). The quantification of differential transcription factor (TF) activity by
166 integrating the RNA- and ATAC-seq data sets revealed key TFs involved in NK cell resistance. We
167 classified TFs as activators (NF2L1, SMRC1, JUN, IRF1 and IRF9) or repressors (RXRB, JUND), based on

168 the expression of the corresponding TF and accessibility of predicted binding sites[25]. STAT1 expression
169 was clearly upregulated but appears to have activating and repressive functions and is therefore
170 classified as undetermined (**Figure 3H**). A closer look at the two top hits *Ly6a* and *Plaat3* showed that
171 both have multiple predicted binding sites for STAT1, IRF1 and IRF9 based on the occurrence of DNA
172 sequence motifs in the vicinity of accessible chromatin (**Figure 3I**). In summary, multiomics analyses
173 revealed that the B-ALL cells, which were not *a priori* sensitive and eliminated by NK cells, showed a
174 highly NK cell-resistant phenotype characterised by a strong IFN-γ signature.

175 ## IFN-γ as major driver of cancer immunoediting

176 The two main functions of NK cells are the direct lysis of tumour cells and the production of pro-
177 apoptotic and -inflammatory cytokines, most importantly IFN-γ. Thus, we aimed to discriminate the
178 relative contributions of killing and cytokine production to cancer immunoediting. To determine the
179 share of direct cytotoxicity, the long-term co-culture experiment was performed with NK cells
180 proficient (WT) or deficient for the pore-forming protein perforin (*Prf1*$^{-/-}$). This deficiency renders them
181 unable to directly kill their target cells[26]. In parallel, B-ALL cells were treated continuously with
182 recombinant IFN-γ. As described above, the growth of GFP^{+} tumour cells was measured by flow
183 cytometry during the experiment. On day 4 and 14, GFP^{+} tumour cells were sorted and co-cultured
184 with freshly prepared WT NK or *Prf1*$^{-/-}$ NK cells or treated continuously with IFN-γ. As previously
185 observed, B-ALL cells co-cultured with WT NK cells showed an initial susceptibility during the first 14
186 days and developed an NK resistance thereafter (**Figure 4A**). As expected, *B2m*$^{-/-}$ B-ALL tumour cells
187 did not survive the co-culture with WT NK cells (**Figure S6A**). In contrast, B-ALL and *B2m*$^{-/-}$ B-ALL cells
188 co-cultured with *Prf1*$^{-/-}$ NK cells or treated with IFN-γ showed a minor but consistent growth inhibition
189 compared to untreated B-ALL cells. This showed that NK cell-derived cytokines, and in particular IFN-
190 γ, had a direct effect on the growth of B-ALL cells (**Figures 4A and S6A**). However, the cytotoxicity assay
191 performed on day 28 after treatment start showed that B-ALL cells continuously treated with IFN-γ
192 were most resistant to WT NK cells (**Figures 4B and S6B**).

193 On day 14, the B-ALL cells were further analysed for their clonal diversity and transcriptomic profiles.
194 In line with our previous experiments, the barcode diversity of the B-ALL + WT NK cell condition was
195 markedly decreased (**Figure 4C**). The tumour cells co-cultured with *Prf1*$^{-/-}$ NK cells or treated with IFN-
196 γ showed a milder decrease of tumour cell diversity (**Figure 4C**). Interestingly, we observed a strong
197 overlap of eliminated and primary resistant tumour cell clones in all three treatment groups, WT NK,
198 *Prf1*$^{-/-}$ NK cell and IFN-γ, suggesting that these cell clones were intrinsically susceptible or resistant to
199 IFN-γ-mediated apoptosis (**Figure 4D**). Apart from the primary resistant tumour cells, we detected cell
200 clones, which acquired resistance due to the NK co-culture or IFN-γ treatment (resistant (2nd)).
201 Strikingly, the number of secondary resistant tumour cell clones was the largest in the B-ALL + WT NK
202 cell condition (n=56 versus 15 and 12 cell clones in B-ALL + *Prf1*$^{-/-}$ NK or IFN-γ, respectively). These
203 findings led us to conclude that NK cells exert an immunological pressure on tumour cells, which is
204 partly independent of IFN-γ production (**Figures 4D&E**). To define the molecular changes driving NK
205 cell resistance in B-ALL cells upon co-culture with WT or *Prf1*$^{-/-}$ NK cells or treatment with IFN-γ, we
206 compared the transcriptomic profiles of all conditions on day 14 after start of treatment. As expected,
207 IFN-γ treatment induced a large number of genes, which overlapped with some of the most significant
208 hits of WT NK and *Prf1*$^{-/-}$ NK cells (23 up- and 10 downregulated genes), such as *Ly6a* and *Plaat3*. We
209 reasoned that changes in gene expression unique for the WT NK cell condition were due to the direct
210 NK cell killing. For instance, we identified an upregulation of *Bnip3*, which was recognised as important
211 player in immune evasion from NK cells before[27]. Additionally, *Aldoa* and *Pgk1* were found to be
212 upregulated, both of which are involved in glycolysis and associated with worse prognosis in
213 pancreatic, cervical and breast cancer[28,29] (**Figures 4F&G and S5**). In conclusion, IFN-γ on the one hand
214 contributed to the selective pressure of NK cells, but on the other hand prolonged IFN-γ exposure led
215 to the dominance of tumour cells that were less sensitive to NK cell attack.

216 Role of PLAAT3 and Ly6A in tumour evasion

217 NK cell resistance in B-ALL cells was associated with altered expression of well-known and novel genes
218 involved in cancer immunoediting. We demonstrated in multiple experiments that *Plaat3* and *Ly6a*

219 belong to the most significantly upregulated genes in NK resistant B-ALL cell lines. Therefore, we
220 decided to follow up on these two genes and unravel their role in immune evasion. We performed the
221 co-culture experiment as described in Figure 4 and analysed the B-ALL cells on day 14 by mass
222 spectrometry to confirm the upregulation of PLAAT3 and Ly6A on the protein level. Indeed, PLAAT3
223 and Ly6A protein expression in B-ALL cells was increased after WT or *Prf1*$^{-/-}$ NK cell co-culture and even
224 more upon IFN-γ treatment (**Figures S7A&5A**). We further generated *Plaat3* KO B-ALL clones by
225 CRISPR/Cas9 genome editing and verified the lack of *Plaat3* mRNA by qPCR (**Figure S7B**). *Plaat3* KO
226 cells did not show any difference in proliferation and viability, IFN-γ production by NK cells and NK
227 receptor ligand expression (**Figures S7C-F**). Moreover, loss of *Plaat3* did not have any impact on direct
228 NK cell-mediated killing of mouse B-ALL cells (**Figure S7G**). To test the relevance of the human
229 orthologue *PLAAT3* in leukaemia, we analysed the *PLAAT3* expression of acute lymphoblastic
230 leukaemia (ALL) patients and observed a trend of worse overall survival in patients with increased
231 *PLAAT3* expression (**Figure S7H**). These results suggest that while PLAAT3 expression is upregulated by
232 IFN-γ and correlates with NK cell resistance, it does not constitute a driver of NK cell resistance.
233 Likewise, we deleted *Ly6a* in B-ALL cells and verified the lack of Ly6A surface protein expression by
234 flow cytometry (**Figure 5B**). Ly6A deficiency had no impact on B-ALL cell proliferation or survival
235 (**Figures 5C&D**). Although IFN-γ production by NK cells as well as surface ligand expression relevant for
236 NK cell interaction was unchanged (**Figures 5E&F**), *Ly6a* KO clones were more susceptible to NK cells
237 compared to WT clones in cytotoxicity assays (**Figure 5G**). This result clearly shows that Ly6A plays an
238 important role in NK immune evasion of mouse B-ALL cells. There are several close orthologues of Ly6A
239 in the human system. Besides a newly described human LY6A/Ly6S gene[30,31], Ly6E and Ly6K have been
240 well-described as close relatives in the human system. We compared the overall survival of ALL
241 patients with a high versus low expression of *LY6E* and *LY6K*, respectively (**Figure 5H&I**). Indeed, a high
242 *LY6E* or *LY6K* expression correlated significantly with poor survival in ALL patients.
243 In summary, our functional analysis of PLAAT3 and Ly6A showed that their expression is upregulated
244 by IFN-γ. Although PLAAT3 was persistently upregulated in our multiomics analysis, it proved not to
245 have any effect on NK cell resistance of the tumour cells. In contrast, Ly6A was identified as a novel

246 driver of tumour evasion from NK cells, by increasing the susceptibility of *Ly6a* deficient tumour cells
247 to NK cells. The poor disease outcome in ALL patients with high *LY6E* and *LY6K* expression supported
248 these findings.

249 Discussion

250 NK cells represent a potent arm of the immune system, tasked with eliminating anomalous cells.
251 Nonetheless, they can fail controlling cancer cells which successfully evaded from the immune
252 surveillance. The presented study aimed to elucidate the evasion mechanisms employed by tumour
253 cells to escape NK cells during initial encounter and extends earlier efforts using patient derived
254 tumour cell lines[10,11,15,32–36]. Notably, patient-derived cell lines have already undergone the cancer
255 immunoediting process and thus have acquired strategies to evade the immune system. On the
256 contrary, our study is based on heterogeneous, non-edited and immune-naïve mouse BCR/ABL^{p185+} B-
257 ALL tumour cell lines. This unique model enables to explore the primary interplay between tumour
258 cells and the immune system. Furthermore, the B-ALL tumour cells have been DNA barcoded, a
259 technique that allows for the quantification of tumour cell clonal dynamics, which can help to better
260 understand the mechanisms of NK cell effector function. To the best of our knowledge, this particular
261 aspect has not been demonstrated in previous studies.
262 We established an *in vitro* model, whereby mouse NK and DNA barcoded B-ALL cells were co-cultured
263 for several days. Transcriptome analysis, assessment of chromatin accessibility and evaluation of clonal
264 evolution were performed at two time points during the experiment. DNA barcoding allowed the
265 determination of tumour cell fate during the co-culture and revealed that most tumour cell clones
266 possessed inherent sensitivity or resistance to NK cells. This technique has already been used by many
267 others to quantify tumour cell susceptibility towards immune cells, drug- or antibody-based
268 immunotherapies[37–40]. Similar to our research, these studies observed that the majority of tumour cells
269 is predestined for being sensitive or resistant to treatment. For instance, Baldwin et al. found pre-
270 existing resistant clones which were positively selected after combined anti-PD1 and anti-CTLA4
271 therapy in mouse mammary cancer and their gene expression signature correlated with worse survival

272 in patients[39]. Our study highlighted tumour cell clones beyond those two fundamental fates of life and
273 death, which acquired secondary resistance in the presence of NK cells. Secondary resistance was only
274 observed in a small subset of tumour cell clones, which showed NK cell resistance in only one of three
275 replicate wells on day 14 of co-culture. Similarly, using DNA barcoding to investigate the clonal
276 evolution of drug-treated lung cancer cells, Acar *et al.* recently described the emergence of "*de novo*
277 resistant lineages" in one replicate only[37]. Interestingly, we found that secondary resistant tumour cells
278 were highly distinctive for each independently performed experiment, suggesting that a stochastic
279 event causes the resistance. This demonstrates that NK cells can shape tumour cells and contribute to
280 immunoediting of tumour cell clones. However, due to the necessity of expanding the barcoded cell
281 lines before the experiments (to ensure reproducible representation of all barcodes in every well), we
282 cannot formally exclude the possibility of pre-existing heterogeneity within a cell clone. Furthermore,
283 the barcode sequence of the LG2.1 library was found to be located approximately 900 bps upstream
284 of the polyA tail and could thus not be detected using single-cell RNA sequencing. It would certainly be
285 interesting to delve deeper into secondary resistance mechanisms and to compare the transcriptomic
286 profiles of primary and secondary resistant tumour cell clones in the future[41,42].
287 We show that NK cells exert immunological pressure on tumour cells, which eventually escape and
288 become refractory to NK cell killing. Amongst others, previously described NK cell tumour evasion
289 mechanisms include the upregulation of proteins involved in antigen presentation and MHC-I and -II
290 molecules[43,44], the loss or shedding of NKG2D ligands such as MHC class I chain-related molecule A and
291 B (MICA/B)[45] and secretion of TGF-β and IL-10[46]. Notably, we here describe *Ly6a* overexpression as
292 emerging novel driver of tumour evasion. Ly6A, also called stem cell antigen-1 (Sca-1), is an 18-kDa
293 mouse glycosyl phosphatidylinositol-anchored cell surface protein. It plays an important role in
294 haematopoietic progenitor/stem cell lineage fate, brain blood barrier transport and cancer stem cell
295 biology[47–50]. Ly6A was shown to be upregulated in cancer stem cells and many tumour entities and is
296 induced by Wnt/β-Catenin signalling and TGF-β deregulation. This promotes cell migration *in vitro,*
297 increased tumourigenicity and resistance to chemotherapy *in vivo*[50–53]. The human LY6 gene family
298 comprises several members, but the direct orthologue of mouse *Ly6a* has been under debate for a

299 long time. Very recently, two independent groups described a novel protein-encoding gene located in
300 region 8q24.3 of the human genome called *LY6A*/*LY6S,* which is upregulated upon IFN-γ treatment and
301 shows high expression in pituitary tumours[30,31]. Previously, other *LY6* family members were suggested
302 as close homologues of the murine Ly6a gene, such as *LY6D*, *LY6E*, *Ly6H* and *LY6K*, which were
303 implicated as novel biomarkers for poor cancer prognosis and are frequently amplified in human
304 cancer[54]. Al Hossiny *et al.* showed that human LY6E and LY6K promote breast cancer *in vivo* and drive
305 drug sensitivity and epithelial-to-mesenchymal transition. Moreover, they observed that LY6E/LY6K
306 are required for TGF-β signalling and facilitate immune evasion by upregulating PD-L1 on cancer cells,
307 by recruiting T-regulatory cells and dampening NK cell activation[55]. In line, our survival analysis of a
308 paediatric ALL-patient cohort confirmed the cancer driving feature of LY6E and LY6K also in leukaemia.
309 Additionally, our results support the observed oncogenic and immune suppressive properties of Ly6A
310 showing that it is highly upregulated after NK cell co-culture and inducible by IFN-γ. Although the exact
311 mechanism remains unknown, the sensitivity towards NK cells increased significantly upon *Ly6a* gene
312 deletion. Our findings align with the notion that immunoedited and thus more aggressive tumour cells
313 may harbour cancer stem cell (CSC) features. CSCs are considered responsible for metastasis and
314 therapy resistance, as they are characterised by deregulated differentiation, self-renewal, drug
315 resistance, and amongst others evasion of immunosurveillance. Unlike other immune cells, NK cells
316 are believed to show direct cytotoxicity against CSCs[56]. On the other hand, as CSCs frequently
317 upregulate classical and non-classical MHC-I molecules while losing NK cell activating ligands, it is still
318 a matter of debate if and how NK cells are able to detect and kill CSCs[56,57].
319 In general, this research underscores the pivotal role of IFN-γ in the acquisition of NK cell resistance
320 and as ultimate driver of immune evasion. In contrast, *in vitro* and *in vivo* gene-editing screens showed
321 that loss of IFN-γ signalling (IFNGR1/2, JAK1/2, etc.) and antigen presentation (B2M, TAP1, etc.) leads
322 to immune evasion from T cells or resistance to immunotherapies[58–60]. However, downregulation of
323 MHC-I converts the tumour cells to prime NK cell targets. It was thus proposed to treat tumours with
324 an NK cell-based therapy to antagonize immune escape from T cells[34]. In our experiments, tumour cells
325 responded to the NK cell co-culture with an upregulation of many IFN-γ inducible genes, such as MHC-

326 I molecules, thereby inhibiting NK cells and inducing resistance. We sought to uncover the role of IFN-
327 γ by comparing the tumour cells co-cultured with WT NK cells to tumour cells treated with IFN-γ. By
328 using DNA barcoding we were able to quantify the effect of IFN-γ on tumour cells and dissect IFN-γ
329 dependent and independent tumour cell fates. We observed that a major part of NK cell susceptible
330 clones overlapped well with the eliminated clones upon IFN-γ treatment (572 of 795 clones). We thus
331 concluded that IFN-γ plays on the one hand a major role in tumour cell elimination and on the other
332 hand enhances NK cell resistance of the remaining tumour cells by upregulating IFN-γ dependent
333 genes, such as genes involved in MHC-I representation and *Ly6a*. The pro-apoptotic functions of IFN-γ
334 have been observed previously in diverse tumour types. IFN-γ signalling was recognised to induce
335 apoptosis-related genes such as caspase 3 and caspase 7 mainly via the JAK/STAT1 pathway[61–64].
336 Although IFN-γ has profound antiproliferative and proapoptotic effects against cancer cells, IFN-γ
337 treatment of cancer patients achieved only minor success probably due to its poor therapeutic index[65].
338 Additionally, it has been proposed that IFN-γ has a dual role in cancer[66]. Its anti- and protumorigenic
339 activities are dependent on the duration (acute versus chronic), magnitude of IFN-γ signalling and the
340 immune cell composition. A deeper understanding of the multifaceted actions of IFN-γ is needed to
341 provide patients the most promising treatment options.
342 In conclusion, our work sheds light on the intricate interplay between NK and leukaemic cells during
343 initial encounters. This study shows that leukaemic cells are actively shaped by NK cells and unravels
344 novel cancer evasion strategies by identifying potential driver genes. Further research, especially *in*
345 *vivo*, is required to delve deeper into the tumour evasion mechanisms involving Ly6A. These findings
346 ultimately deepen our understanding of the initial interaction of tumour and NK cells and eventual
347 cancer immune evasion.

348 ## References:

349 1. Gubin, M. M. & Vesely, M. D. Cancer Immunoediting in the Era of Immuno-oncology. *Clin. Cancer*
350 *Res.* **28**, 3917–3928 (2022).
351 2. Dunn, G. P., Bruce, A. T., Ikeda, H., Old, L. J. & Schreiber, R. D. Cancer immunoediting: from
352 immunosurveillance to tumor escape. *Nat. Immunol.* **3**, 991–998 (2002).
353 3. Wolf, N. K., Kissiov, D. U. & Raulet, D. H. Roles of natural killer cells in immunity to cancer, and
354 applications to immunotherapy. *Nat. Rev. Immunol.* **23**, 90–105 (2023).
355 4. Metkar, S. S. *et al.* Cytotoxic Cell Granule-Mediated Apoptosis: Perforin Delivers Granzyme B-
356 Serglycin Complexes into Target Cells without Plasma Membrane Pore Formation. *Immunity* **16**,
357 417–428 (2002).
358 5. Prager, I. & Watzl, C. Mechanisms of natural killer cell-mediated cellular cytotoxicity. *J. Leukoc.*
359 *Biol.* **105**, 1319–1329 (2019).
360 6. Wang, W. NK cell-mediated antibody-dependent cellular cytotoxicity in cancer immunotherapy.
361 *Front. Immunol.* **6**, (2015).
362 7. Huntington, N. D., Cursons, J. & Rautela, J. The cancer–natural killer cell immunity cycle. *Nat. Rev.*
363 *Cancer* **20**, 437–454 (2020).
364 8. Bald, T., Krummel, M. F., Smyth, M. J. & Barry, K. C. The NK cell–cancer cycle: advances and new
365 challenges in NK cell–based immunotherapies. *Nat. Immunol.* **21**, 835–847 (2020).
366 9. Liu, E. *et al.* Use of CAR-Transduced Natural Killer Cells in CD19-Positive Lymphoid Tumors. *N. Engl.*
367 *J. Med.* **382**, 545–553 (2020).
368 10. Bernareggi, D. *et al.* CHMP2A regulates tumor sensitivity to natural killer cell-mediated
369 cytotoxicity. *Nat. Commun.* **13**, 1899 (2022).
370 11. Chiba, M. *et al.* Genome-wide CRISPR screens identify CD48 defining susceptibility to NK
371 cytotoxicity in peripheral T-cell lymphomas. *Blood* **140**, 1951–1963 (2022).
372 12. Pech, M. F. *et al.* Systematic identification of cancer cell vulnerabilities to natural killer cell-
373 mediated immune surveillance. *eLife* **8**, e47362 (2019).

374 13. Sheffer, M. *et al.* Genome-scale screens identify factors regulating tumor cell responses to natural
375 killer cells. *Nat. Genet.* **53**, 1196–1206 (2021).
376 14. Carré, T. *et al.* Selection of tumor-resistant variants following sustained natural killer cell-mediated
377 immune stress. *Oncol. Rep.* **45**, 582–594 (2021).
378 15. Dufva, O. *et al.* Single-cell functional genomics reveals determinants of sensitivity and resistance
379 to natural killer cells in blood cancers. *Immunity* **56**, 2816-2835.e13 (2023).
380 16. Naik, S. H., Schumacher, T. N. & Perié, L. Cellular barcoding: A technical appraisal. *Exp. Hematol.*
381 **42**, 598–608 (2014).
382 17. Eisele, A. S. *et al.* Erythropoietin directly remodels the clonal composition of murine hematopoietic
383 multipotent progenitor cells. *eLife* **11**, e66922 (2020).
384 18. Marsolier, J. *et al.* H3K27me3 conditions chemotolerance in triple-negative breast cancer. *Nat.*
385 *Genet.* **54**, 459–468 (2022).
386 19. Kärre, K., Ljunggren, H. G., Piontek, G. & Kiessling, R. Selective rejection of H–2-deficient lymphoma
387 variants suggests alternative immune defence strategy. *Nature* **319**, 675–678 (1986).
388 20. Naik, S. H. *et al.* Diverse and heritable lineage imprinting of early haematopoietic progenitors.
389 *Nature* **496**, 229–32 (2013).
390 21. Eisele, A. S. *et al.* Erythropoietin directly remodels the clonal composition of murine hematopoietic
391 multipotent progenitor cells. *eLife* **11**, e66922 (2022).
392 22. Bai, R. *et al.* Mechanisms of Cancer Resistance to Immunotherapy. *Front. Oncol.* **10**, 1290 (2020).
393 23. Sharma, P., Hu-Lieskovan, S., Wargo, J. A. & Ribas, A. Primary, Adaptive, and Acquired Resistance
394 to Cancer Immunotherapy. *Cell* **168**, 707–723 (2017).
395 24. Zhou, F. Molecular Mechanisms of IFN-γ to Up-Regulate MHC Class I Antigen Processing and
396 Presentation. *Int. Rev. Immunol.* **28**, 239–260 (2009).
397 25. Berest, I. *et al.* Quantification of Differential Transcription Factor Activity and Multiomics-Based
398 Classification into Activators and Repressors: diffTF. *Cell Rep.* **29**, 3147-3159.e12 (2019).
399 26. Kägi, D. *et al.* Cytotoxicity mediated by T cells and natural killer cells is greatly impaired in perforin-
400 deficient mice. *Nature* **369**, 31–37 (1994).

401 27. Macher-Goeppinger, S. *et al.* Expression and Functional Characterization of the BNIP3 Protein in
402 Renal Cell Carcinomas. *Transl. Oncol.* **10**, 869–875 (2017).
403 28. Ji, S. *et al.* ALDOA functions as an oncogene in the highly metastatic pancreatic cancer. *Cancer Lett.*
404 **374**, 127–135 (2016).
405 29. He, Y. *et al.* PGK1-mediated cancer progression and drug resistance. *Am. J. Cancer Res.* **9**, 2280–
406 2302 (2019).
407 30. Liu, D. *et al.* A systematic survey of LU domain-containing proteins reveals a novel human gene,
408 LY6A, which encodes the candidate ortholog of mouse Ly-6A/Sca-1 and is aberrantly expressed in
409 pituitary tumors. *Front. Med.* (2023) doi:10.1007/s11684-022-0968-4.
410 31. Shmerling, M. *et al.* LY6S, a New IFN-Inducible Human Member of the Ly6a Subfamily Expressed
411 by Spleen Cells and Associated with Inflammation and Viral Resistance. *ImmunoHorizons* **6**, 253–
412 272 (2022).
413 32. Pech, M. F. *et al.* Systematic identification of cancer cell vulnerabilities to natural killer cell-
414 mediated immune surveillance. *eLife* **8**, e47362 (2019).
415 33. Zhuang, X., Veltri, D. P. & Long, E. O. Genome-Wide CRISPR Screen Reveals Cancer Cell Resistance
416 to NK Cells Induced by NK-Derived IFN-γ. *Front. Immunol.* **10**, (2019).
417 34. Freeman, A. J. *et al.* Natural Killer Cells Suppress T Cell-Associated Tumor Immune Evasion. *Cell*
418 *Rep.* **28**, 2784-2794.e5 (2019).
419 35. Sheffer, M. *et al.* Genome-scale screens identify factors regulating tumor cell responses to natural
420 killer cells. *Nat. Genet.* **53**, 1196–1206 (2021).
421 36. Dubrot, J. *et al.* In vivo CRISPR screens reveal the landscape of immune evasion pathways across
422 cancer. *Nat. Immunol.* **23**, 1495–1506 (2022).
423 37. Acar, A. *et al.* Exploiting evolutionary steering to induce collateral drug sensitivity in cancer. *Nat.*
424 *Commun.* **11**, 1923 (2020).
425 38. Umkehrer, C. *et al.* Isolating live cell clones from barcoded populations using CRISPRa-inducible
426 reporters. *Nat. Biotechnol.* **39**, 174–178 (2021).

39. Baldwin, L. A. *et al.* DNA barcoding reveals ongoing immunoediting of clonal cancer populations during metastatic progression and immunotherapy response. *Nat. Commun.* **13**, 6539 (2022).
40. Goyal, Y. *et al.* Diverse clonal fates emerge upon drug treatment of homogeneous cancer cells. *Nature* **620**, 651–659 (2023).
41. Weinreb, C., Rodriguez-Fraticelli, A., Camargo, F. D. & Klein, A. M. Lineage tracing on transcriptional landscapes links state to fate during differentiation. *Science* **367**, eaaw3381 (2020).
42. Chang, M. T. *et al.* Identifying transcriptional programs underlying cancer drug response with TraCe-seq. *Nat. Biotechnol.* **40**, 86–93 (2022).
43. Ljunggren, H.G. & Kärre, K. In serach of the 'missing self': MHC molecules and NK cell recognition. *Immunol. Today* **11**, 237–244 (1990).
44. Weichold, F. F. *et al.* Regulation of a Graft-Versus-Leukemia Effect by Major Histocompatibility Complex Class II Molecules on Leukemia Cells: HLA-DR1 Expression Renders K562 Cell Tumors Resistant to Adoptively Transferred Lymphocytes in Severe Combined Immunodeficiency Mice/Nonobese Diabetic Mice. *Blood* **90**, 4553–4558 (1997).
45. Xing, S. & Ferrari de Andrade, L. NKG2D and MICA/B shedding: a 'tag game' between NK cells and malignant cells. *Clin. Transl. Immunol.* **9**, e1230 (2020).
46. Konjević, G. M., Vuletić, A. M., Mirjačić Martinović, K. M., Larsen, A. K. & Jurišić, V. B. The role of cytokines in the regulation of NK cells in the tumor environment. *Cytokine* **117**, 30–40 (2019).
47. Holmes, C. & Stanford, W. L. Concise Review: Stem Cell Antigen-1: Expression, Function, and Enigma. *Stem Cells* **25**, 1339–1347 (2007).
48. Bradfute, S. B., Graubert, T. A. & Goodell, M. A. Roles of Sca-1 in hematopoietic stem/progenitor cell function. *Exp. Hematol.* **33**, 836–843 (2005).
49. Hordeaux, J. *et al.* The GPI-Linked Protein LY6A Drives AAV-PHP.B Transport across the Blood-Brain Barrier. *Mol. Ther.* **27**, 912–921 (2019).
50. Park, J. W., Park, J. M., Park, D. M., Kim, D.-Y. & Kim, H. K. Stem Cells Antigen-1 Enriches for a Cancer Stem Cell-Like Subpopulation in Mouse Gastric Cancer. *Stem Cells* **34**, 1177–1187 (2016).

453 51. Li, Y. *et al.* Evidence that transgenes encoding components of the Wnt signaling pathway
454 preferentially induce mammary cancers from progenitor cells. *Proc. Natl. Acad. Sci. U. S. A.* **100**,
455 15853–15858 (2003).
456 52. Roarty, K., Baxley, S. E., Crowley, M. R., Frost, A. R. & Serra, R. Loss of TGF-β or Wnt5a results in an
457 increase in Wnt/β-catenin activity and redirects mammary tumour phenotype. *Breast Cancer Res.*
458 *BCR* **11**, R19 (2009).
459 53. Batts, T. D. *et al.* Stem Cell Antigen-1 (Sca-1) Regulates Mammary Tumor Development and Cell
460 Migration. *PLOS ONE* **6**, e27841 (2011).
461 54. Luo, L. *et al.* Distinct lymphocyte antigens 6 (Ly6) family members Ly6D, Ly6E, Ly6K and Ly6H drive
462 tumorigenesis and clinical outcome. *Oncotarget* **7**, 11165–11193 (2016).
463 55. Al Hossiny, M. *et al.* Ly6E/K signaling to TGF-β promotes breast cancer progression, immune
464 escape and drug resistance. *Cancer Res.* **76**, 3376–3386 (2016).
465 56. Shokouhifar, A., Firouzi, J., Nouri, M., Sarab, G. A. & Ebrahimi, M. NK cell upraise in the dark world
466 of cancer stem cells. *Cancer Cell Int.* **21**, 682 (2021).
467 57. Tsuchiya, H. & Shiota, G. Immune evasion by cancer stem cells. *Regen. Ther.* **17**, 20–33 (2021).
468 58. Pan, D. *et al.* A major chromatin regulator determines resistance of tumor cells to T cell–mediated
469 killing. *Science* **359**, 770–775 (2018).
470 59. Manguso, R. T. *et al.* In vivo CRISPR screening identifies Ptpn2 as a cancer immunotherapy target.
471 *Nature* **547**, 413–418 (2017).
472 60. Cucolo, L. *et al.* The interferon-stimulated gene RIPK1 regulates cancer cell intrinsic and extrinsic
473 resistance to immune checkpoint blockade. *Immunity* **55**, 671-685.e10 (2022).
474 61. Song, M. *et al.* Low-Dose IFNγ Induces Tumor Cell Stemness in Tumor Microenvironment of Non-
475 Small Cell Lung Cancer. *Cancer Res.* **79**, 3737–3748 (2019).
476 62. Hao, Q. & Tang, H. Interferon-γ and Smac mimetics synergize to induce apoptosis of lung cancer
477 cells in a TNFα-independent manner. *Cancer Cell Int.* **18**, 84 (2018).
478 63. Su, Q., Wang, F., Dong, Z., Chen, M. & Cao, R. IFN-γ induces apoptosis in human melanocytes by
479 activating the JAK1/STAT1 signaling pathway. *Mol. Med. Rep.* **22**, 3111–3116 (2020).

480 64. Sironi, J. J. & Ouchi, T. STAT1-induced Apoptosis Is Mediated by Caspases 2, 3, and 7 *. *J. Biol.*
481 *Chem.* **279**, 4066–4074 (2004).
482 65. Shen, J. *et al.* Anti-cancer therapy with TNFα and IFNγ: A comprehensive review. *Cell Prolif.* **51**,
483 e12441 (2018).
484 66. Zaidi, M. R. The Interferon-Gamma Paradox in Cancer. *J. Interferon Cytokine Res.* **39**, 30–38 (2019).
485 67. ClustVis: a web tool for visualizing clustering of multivariate data using Principal Component
486 Analysis and heatmap | Nucleic Acids Research | Oxford Academic.
487 https://academic.oup.com/nar/article/43/W1/W566/2467929.
488 68. Federico, A. & Monti, S. hypeR: an R package for geneset enrichment workflows. *Bioinformatics*
489 **36**, 1307–1308 (2019).
490 69. Berest, I. *et al.* Quantification of Differential Transcription Factor Activity and Multiomics-Based
491 Classification into Activators and Repressors: diffTF. *Cell Rep.* **29**, 3147-3159.e12 (2019).
492 70. Kulakovskiy, I. V. *et al.* HOCOMOCO: expansion and enhancement of the collection of transcription
493 factor binding sites models. *Nucleic Acids Res.* **44**, D116–D125 (2016).
494 71. Zijlstra, M. *et al.* Beta 2-microglobulin deficient mice lack CD4-8+ cytolytic T cells. *Nature* **344**, 742–
495 746 (1990).
496 72. Dull, T. *et al.* A Third-Generation Lentivirus Vector with a Conditional Packaging System. *J. Virol.*
497 **72**, 8463–8471 (1998).
498 73. Pagès, H., Aboyoun, R., Gentleman, R., & DebRoy, S. Biostrings: Efficient manipulation of biological
499 strings version 2.58.0 from Bioconductor. https://rdrr.io/bioc/Biostrings/ (2020).
500 74. Love, M. I., Huber, W. & Anders, S. Moderated estimation of fold change and dispersion for RNA-
501 seq data with DESeq2. *Genome Biol.* **15**, 550 (2014).
502 75. Mölder, F. *et al.* Sustainable data analysis with Snakemake. *F1000Research* **10**, 33 (2021).
503 76. Dobin, A. *et al.* STAR: ultrafast universal RNA-seq aligner. *Bioinformatics* **29**, 15–21 (2013).
504 77. Patro, R., Duggal, G., Love, M. I., Irizarry, R. A. & Kingsford, C. Salmon: fast and bias-aware
505 quantification of transcript expression using dual-phase inference. *Nat. Methods* **14**, 417–419
506 (2017).

507 78. Zhu, A., Ibrahim, J. G. & Love, M. I. Heavy-tailed prior distributions for sequence count data:
508 removing the noise and preserving large differences. *Bioinformatics* **35**, 2084–2092 (2019).
509 79. Ritchie, M. E. *et al.* limma powers differential expression analyses for RNA-sequencing and
510 microarray studies. *Nucleic Acids Res.* **43**, e47 (2015).
511 80. Liberzon, A. *et al.* The Molecular Signatures Database (MSigDB) hallmark gene set collection. *Cell*
512 *Syst.* **1**, 417–425 (2015).
513 81. Buenrostro, J. D., Wu, B., Chang, H. Y. & Greenleaf, W. J. ATAC-seq: A Method for Assaying
514 Chromatin Accessibility Genome-Wide. *Curr. Protoc. Mol. Biol.* **109**, (2015).
515 82. Ewels, P. A. *et al.* The nf-core framework for community-curated bioinformatics pipelines. *Nat.*
516 *Biotechnol.* **38**, 276–278 (2020).
517 83. Gaspar, J. M. Improved peak-calling with MACS2. 496521 Preprint at
518 https://doi.org/10.1101/496521 (2018).
519 84. Heinz, S. *et al.* Simple combinations of lineage-determining transcription factors prime cis-
520 regulatory elements required for macrophage and B cell identities. *Mol. Cell* **38**, 576–589 (2010).
521 85. Quinlan, A. R. & Hall, I. M. BEDTools: a flexible suite of utilities for comparing genomic features.
522 *Bioinforma. Oxf. Engl.* **26**, 841–842 (2010).
523 86. Liao, Y., Smyth, G. K. & Shi, W. featureCounts: an efficient general purpose program for assigning
524 sequence reads to genomic features. *Bioinformatics* **30**, 923–930 (2014).
525 87. Thorvaldsdóttir, H., Robinson, J. T. & Mesirov, J. P. Integrative Genomics Viewer (IGV): high-
526 performance genomics data visualization and exploration. *Brief. Bioinform.* **14**, 178–192 (2013).
527 88. Ewels, P., Magnusson, M., Lundin, S. & Käller, M. MultiQC: summarize analysis results for multiple
528 tools and samples in a single report. *Bioinformatics* **32**, 3047–3048 (2016).
529 89. Wiśniewski, J. R., Zougman, A., Nagaraj, N. & Mann, M. Universal sample preparation method for
530 proteome analysis. *Nat. Methods* **6**, 359–362 (2009).
531 90. Block, J. *et al.* Systemic Inflammation and Normocytic Anemia in DOCK11 Deficiency. *N. Engl. J.*
532 *Med.* (2023) doi:10.1056/NEJMoa2210054.
533

534 # Figures

Figure 1

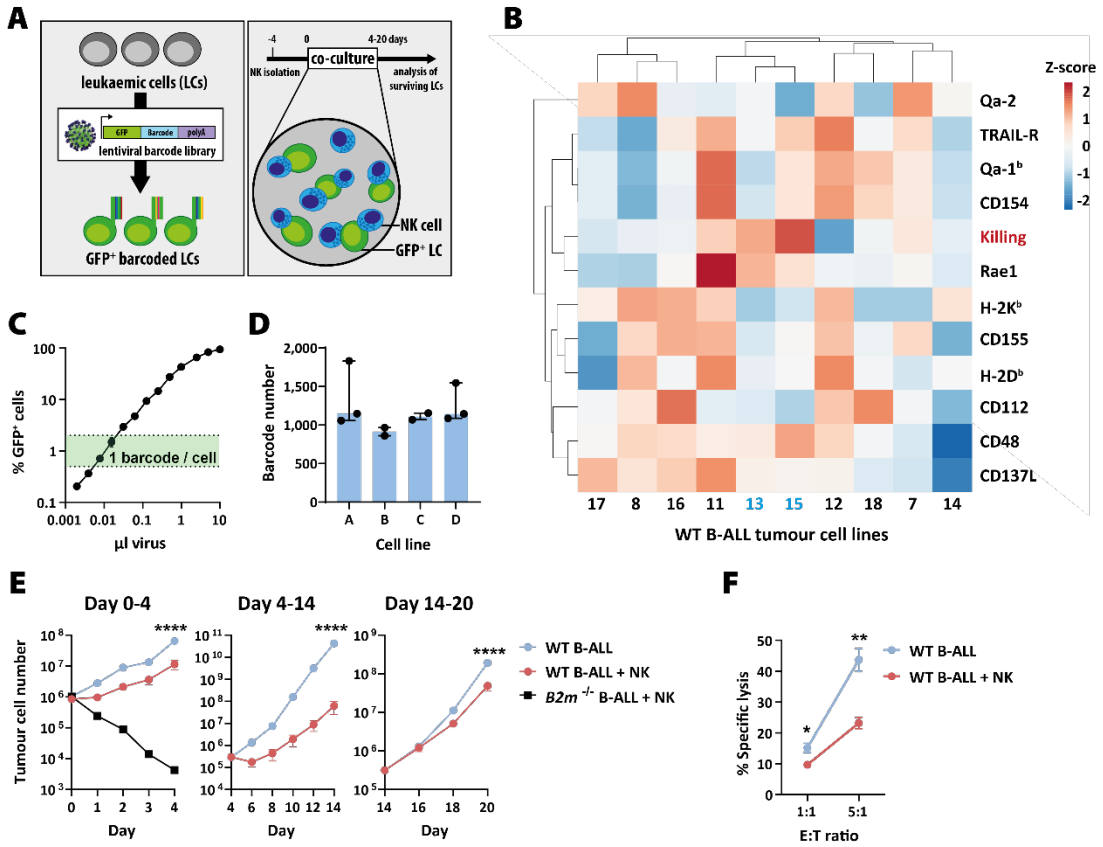

535

536 **Figure 1: Co-culture system to study cancer immunoediting *in vitro*. (A)** Scheme illustrates the
537 experimental setup: BCR/ABL^{p185+} B-ALL leukaemic cells (LCs) are transduced with a DNA barcode
538 library. Barcoded LCs are co-cultured with NK cells for 4-20 days *in vitro*. **(B)** Ten B-ALL cell lines were
539 generated from C57BL/6 WT mice and characterised regarding the surface expression of NK ligands
540 (black) and their susceptibility towards NK cell killing (red, depicted here is the cytotoxicity at E:T=10:1)
541 measured by flow cytometry. Cell lines #13 and #15, in blue, showed the highest NK cell susceptibility
542 and were used for the following experiments. Rows were centered; unit variance scaling was applied
543 to rows. Both rows and columns were clustered using correlation distance and average linkage. The
544 plot was generated using the Clustvis web tool[67]. **(C)** B-ALL cell lines were DNA barcoded by lentiviral
545 transduction. Using different amounts of viral supernatant, the optimum transduction efficiency
546 (<5%)[16] was chosen to allow a single barcode integration per cell as determined by GFP expression and
547 measured by flow cytometry. Shown are means±SD (n=2) of one representative cell line. **(D)** Cell lines

548 A-D were analysed for their barcode diversity. Two B-ALL cell lines (#13 and #15) were barcoded (n=2
549 independent transductions, <5% transduction efficiency) and the barcode diversity of the FACS-
550 purified GFP^+ cell lines was determined by targeted DNA sequencing. Cell lines A and B were derived
551 from #13 and cell lines C and D from #15. Bars show barcode diversity of barcoded tumour cell lines
552 (A&D n=3 and B&C n=2 independent experiments, each determined by sequencing of 3 biological and
553 2 technical replicates). Shown is median with interquartile range. **(E)** Barcoded WT B-ALL cell lines A-D
554 (n=4) were cultivated in three individual wells either in the absence or presence of purified and IL-2-
555 activated NK cells. One *B2m*$^{-/-}$ B-ALL cell line was included as control. Absolute numbers of B-ALL cells
556 were determined by flow cytometry. On day 0, 4 and 14, B-ALL cells were FACS sorted, re-plated and
557 fresh NK cells were replenished. Shown are means±SD of n=4 B-ALL cell lines of one representative
558 experiment (n=3 independent experiments); the significance was calculated by an unpaired t-test. **(F)**
559 On day 29, a standard 4h NK cytotoxicity assay was performed using B-ALL cells that had been cultured
560 for 20 days in the presence or absence of NK cells. Shown are means±SEM of n=4 cell lines (in technical
561 triplicates) of one representative experiment (n=3 experiments); the significance was calculated by a
562 paired t-test.

Figure 2

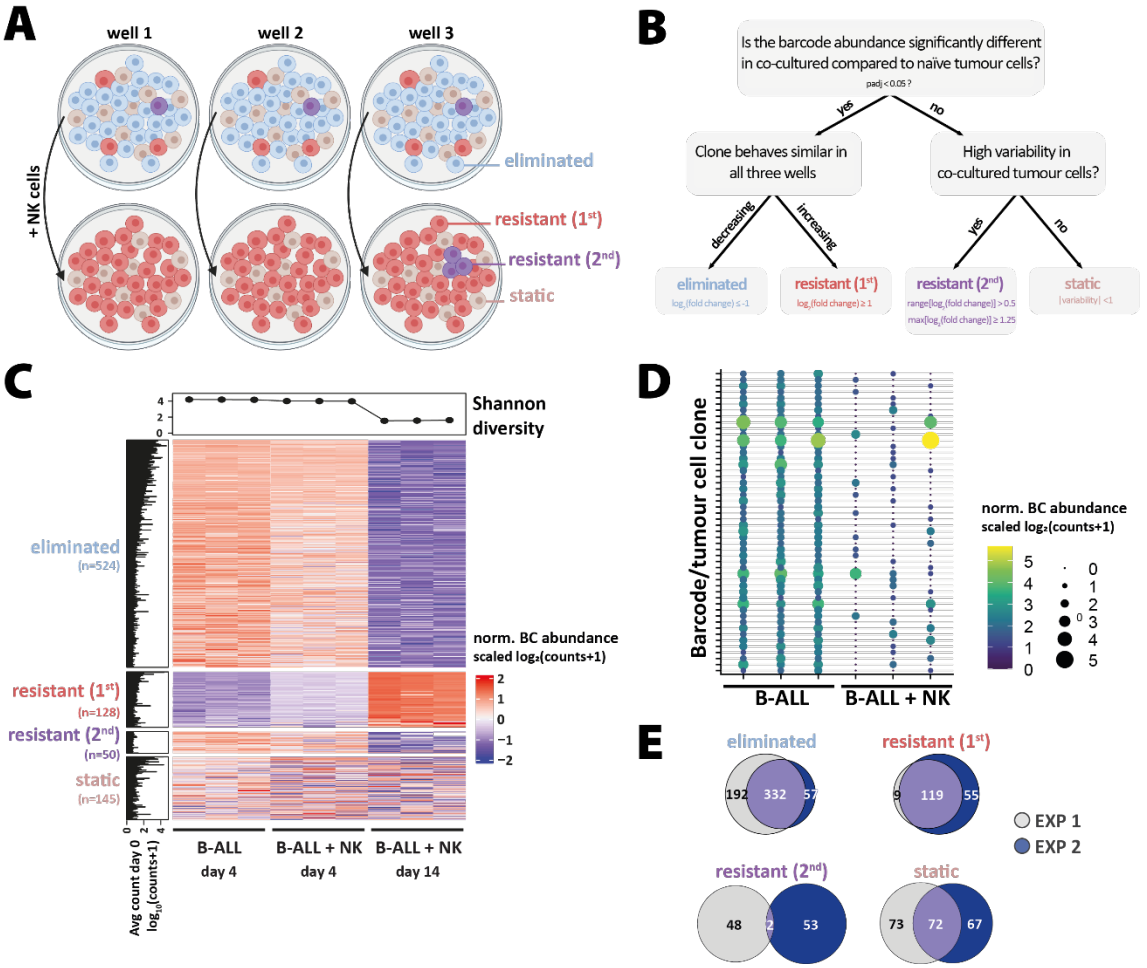

Figure 2: Quantification of NK cell-mediated cancer immunoediting *in vitro*. (A-B) Schematic representation of the proposed model. Upon long-term co-culture of B-ALL and NK cells, we hypothesised that each tumour cell clone would fall in one of the following categories: The abundance of the clone can be significantly higher (primary resistant) or lower (eliminated), unchanged (static) or show a high variability (secondary resistant). **(B)** A rule-based decision tree was designed to discriminate the four categories depicted in (A). Variability is defined as $v = log2(max(x + 1)/min(x + 1))$, where x is a vector of normalised counts across samples. **(C)** The heatmap shows the normalised abundance of barcodes (norm. BC abundance) of cell line A (n=3 wells) from one representative experiment (in total: n=4 cell lines, n=2 experiments, n=3 wells, sequenced in technical duplicates). Each column in the figure represents a sample (well), and each row represents a barcode. The barcodes were divided into the four pre-defined groups according to the criteria defined in (B). The Shannon index (shown above the heatmap) serves as measure of barcode diversity and drops

576 significantly after 14 days of NK co-culture. The histogram on the left shows the average abundance of
577 the barcoded cell clone in the B-ALL only samples on day 4. **(D)** The bubble plot depicts the normalised
578 abundance of barcodes of resistant (2nd) clones in B-ALL samples (day 4) compared to B-ALL + NK
579 samples (day 14). The size and colour of the bubbles indicate the normalised barcode abundance.
580 Shown here is the same cell line and experiment as in (C). **(E)** Comparing two individual experiments
581 using the same representative cell line A as shown in (C&D), the Euler diagrams highlight a high overlap
582 of eliminated, resistant (1st), and static cell clones. In contrast, only two resistant (2nd) clones were
583 shared between both independent experiments.

Figure 3

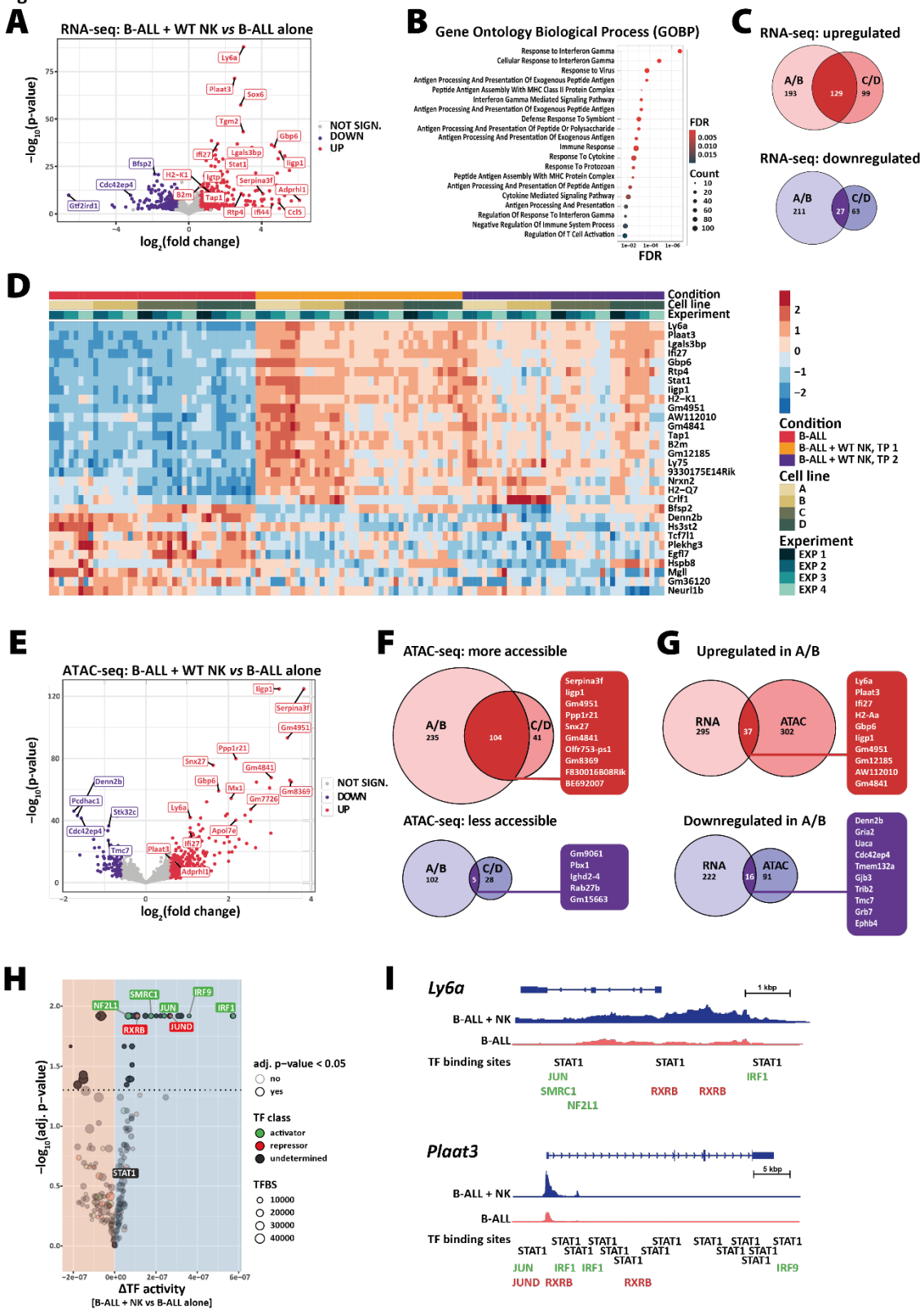

Figure 3: Integrative analysis of RNA-seq and ATAC-seq shows well-known and novel genes deregulated in NK resistant B-ALL cells. The transcriptome **(A-D and G)** and chromatin accessibility **(E-I)** analysis of B-ALL cells co-cultured with NK cells for 4 (time point 1 (TP1)) or 14 (TP2) days were

588 analysed and compared to the non-co-cultured B-ALL cells on TP1 (n=3-4 independent experiments).
589 **(A)** The volcano plot shows the significantly up- or downregulated genes in B-ALL cell lines A and B
590 after co-culture with NK cells for 14 days (n=3 experiments). Statistics were calculated with the Wald
591 test (adjusted p-value (padj)_cutoff < 0.05; log_2FC_cutoff > 0.58 (FC = 2)). **(B)** The dot plot illustrates
592 the enrichment analysis using the hyperR tool[68] for the Gene Ontology Biological Process (GOBP) terms
593 associated with NK co-cultured B-ALL cells shown in panel (A). X-axis and dot colour depicts the false
594 discovery rate (FDR) and y-axis the corresponding biological processes. Dot size illustrates the number
595 of genes associated with the biological processes. **(C)** The Euler diagrams display up- or downregulated
596 genes in cell lines A/B and/or C/D after 14 days of NK co-culture. **(D)** Heatmap shows the expression
597 of selected overlapping genes (top-20 up-regulated, top-10 down-regulated; ranked by p-value)
598 identified in (C) (n=3-4 experiments, 4 B-ALL cell lines). The row-scaled normalized counts represent
599 the log_2(fold change). **(E)** The volcano plot shows differentially accessible chromatin regions in B-ALL
600 cells A and B after co-culture with NK cells for 14 days (n=3 experiments). Statistics were calculated
601 with the Wald test (padj_cutoff < 0.05; log_2FC_cutoff > 0.58 (FC = 2)). **(F)** The Euler diagrams highlight
602 genes whose promoters (TSS +/- 3kb) had higher or lower chromatin accessibility in cell lines A/B
603 and/or C/D after 14 days of NK co-culture in n=3-4 experiments. Gene promoters with the highest
604 |log_2(fold change)| are highlighted. **(G)** Integration of RNA- and ATAC-seq data shows that 37 genes
605 are up- and 16 downregulated in cell lines A/B; the top 10 up- or downregulated genes are highlighted
606 on the right. **(H)** Differential transcription factors (diffTF) analysis[69] highlighted activator (green) and
607 repressor (red) transcription factors (TFs) that were differentially expressed in B-ALL cell lines A and B
608 after NK co-culture (right side of the plot) or B-ALL alone (left side of the plot). **(I)** Integrative Genomics
609 Viewer (IGV) genome browser tracks display representative ATAC-seq signal densities at the *Ly6a* and
610 *Plaat3* loci in B-ALL cells with or without NK co-culture. Shown are the gene bodies including a 3 kb
611 upstream promoter region, as well as binding sites of TFs identified in (H). Database HOCOMOCO
612 (v10)[70] was used and depicted are counts per million (CPM) with a range of [0-1.37].

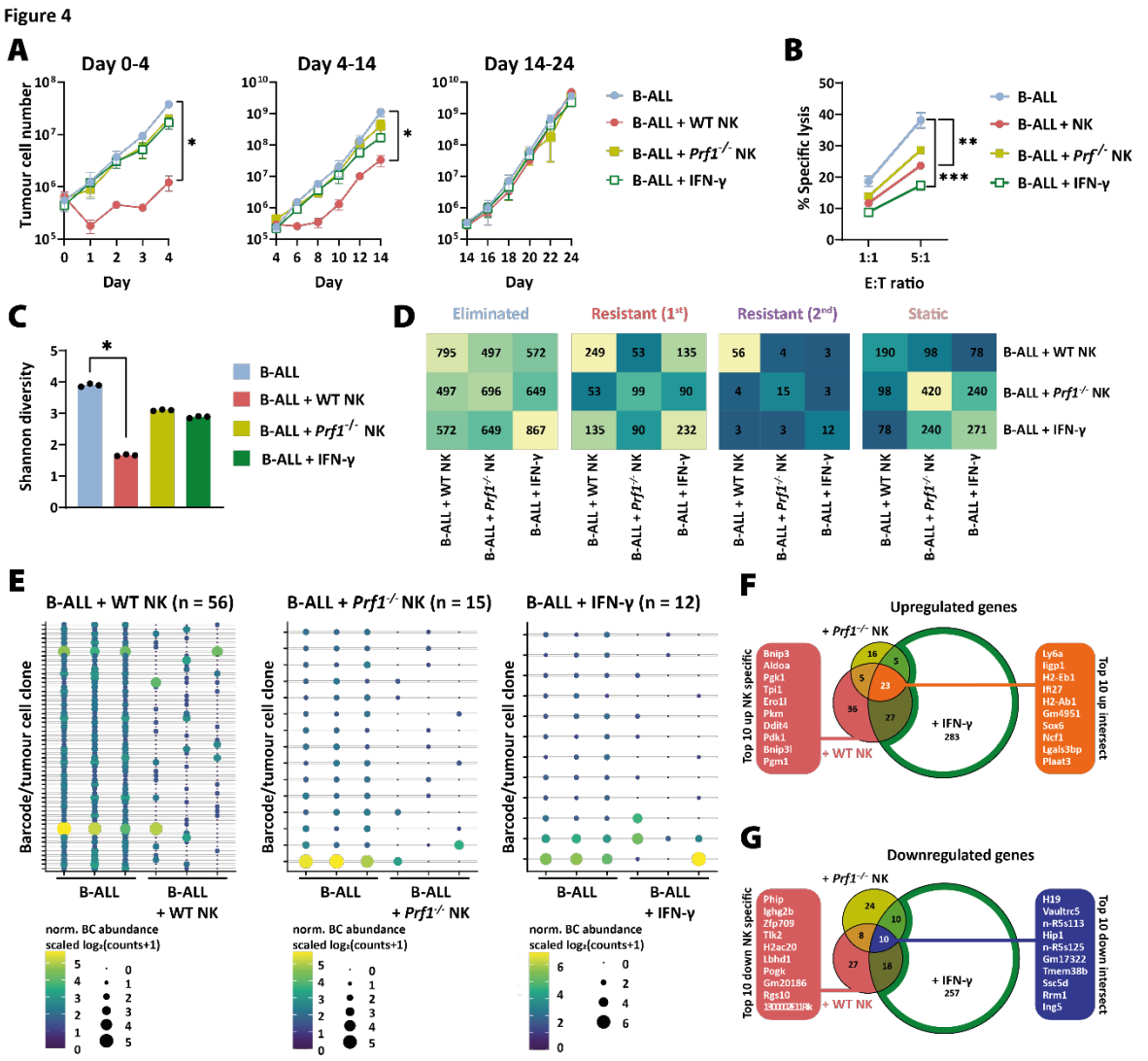

613

614 **Figure 4: NK cell-derived IFN-γ is a major driver of leukaemia immunoediting. (A)** Barcoded WT B-ALL
615 cell lines (n=2 cell lines A&D) were cultivated in three individual wells either in the absence or presence
616 of purified and IL-2-activated WT or *Prf1*$^{-/-}$ NK cells or with 2 ng/ml IFN-γ. Absolute numbers of B-ALL
617 cells were determined by flow cytometry. On day 0, 4 and 14, B-ALL cells were FACS sorted, re-plated
618 and fresh NK cells were replenished. Shown are means±SD of n=2 B-ALL cell lines of one representative
619 experiment (n=2 independent experiments). The significance was calculated with the Kruskal-Wallis
620 test and Dunn´s multiple comparisons testing. **(B)** On day 28, a standard 4h NK cytotoxicity assay with
621 WT NK cells was performed using B-ALL cells that had been cultured for 27 days in the presence or
622 absence of NK cells or IFN-γ. Shown are means±SEM of 2 cell lines (in technical triplicates) of one
623 representative experiment (n=2 experiments). Statistics were calculated with a matched two-way

624 ANOVA with Dunnett´s multiple comparisons test. **(C)** B-ALL cells were FACS sorted on day 14, and the
625 barcode diversity was determined by targeted DNA amplicon sequencing. The Shannon diversity of
626 leukaemic clones dropped significantly ($p = 0.0134$) upon co-culture with WT NK cells, and to a lesser
627 degree with *Prf1*$^{-/-}$ NK cells or recombinant IFN-γ. Shown is the mean and dots depict each replicate.
628 Statistics were calculated with the Kruskal-Wallis and Dunn´s multiple comparisons testing. **(D)** The
629 barcodes within each sample were classified according to the decision tree in Fig. 2B. The barcodes
630 that were attributed to the four pre-defined groups were compared between the treatment groups.
631 Heatmaps indicate the number of barcodes shared between treatment groups (bright yellow = high,
632 dark green = low). Resistant (1st) and eliminated leukaemic clones were broadly overlapping between
633 WT or *Prf1*$^{-/-}$ NK- or IFN-γ-treated B-ALL cells. However, resistant (2nd) leukaemic clones were highly
634 specific for each of these conditions. **(E)** The bubble plots show the normalised abundance of barcodes
635 of resistant (2nd) clones in B-ALL samples compared to B-ALL + WT or *Prf1*$^{-/-}$ NK or IFN-γ samples (day
636 14). The size and colour of the bubbles indicate the barcode abundance. **(F)** The Euler diagram displays
637 the number up-regulated genes in cell lines A/D after 14 days of co-culture with WT or *Prf1*$^{-/-}$ NK cells
638 or stimulation with recombinant IFN-γ. The orange list highlights the top 10 upregulated genes in the
639 intersection of the three comparisons and the red list shows the WT NK cell specific top 10 upregulated
640 genes. **(G)** The Euler diagram displays the number of downregulated genes in cell lines A/D after 14
641 days of co-culture with WT or *Prf1*$^{-/-}$ NK cells or stimulation with recombinant IFN-γ. The blue list
642 highlights the top 10 downregulated genes in the intersection of the three comparisons and the red
643 list shows the WT NK cell specific top 10 downregulated genes. (A-G) Shown is one representative
644 experiment (A&B, n=2 cell lines) or one representative cell line from one experiment (C-G, n=2 cell
645 lines).

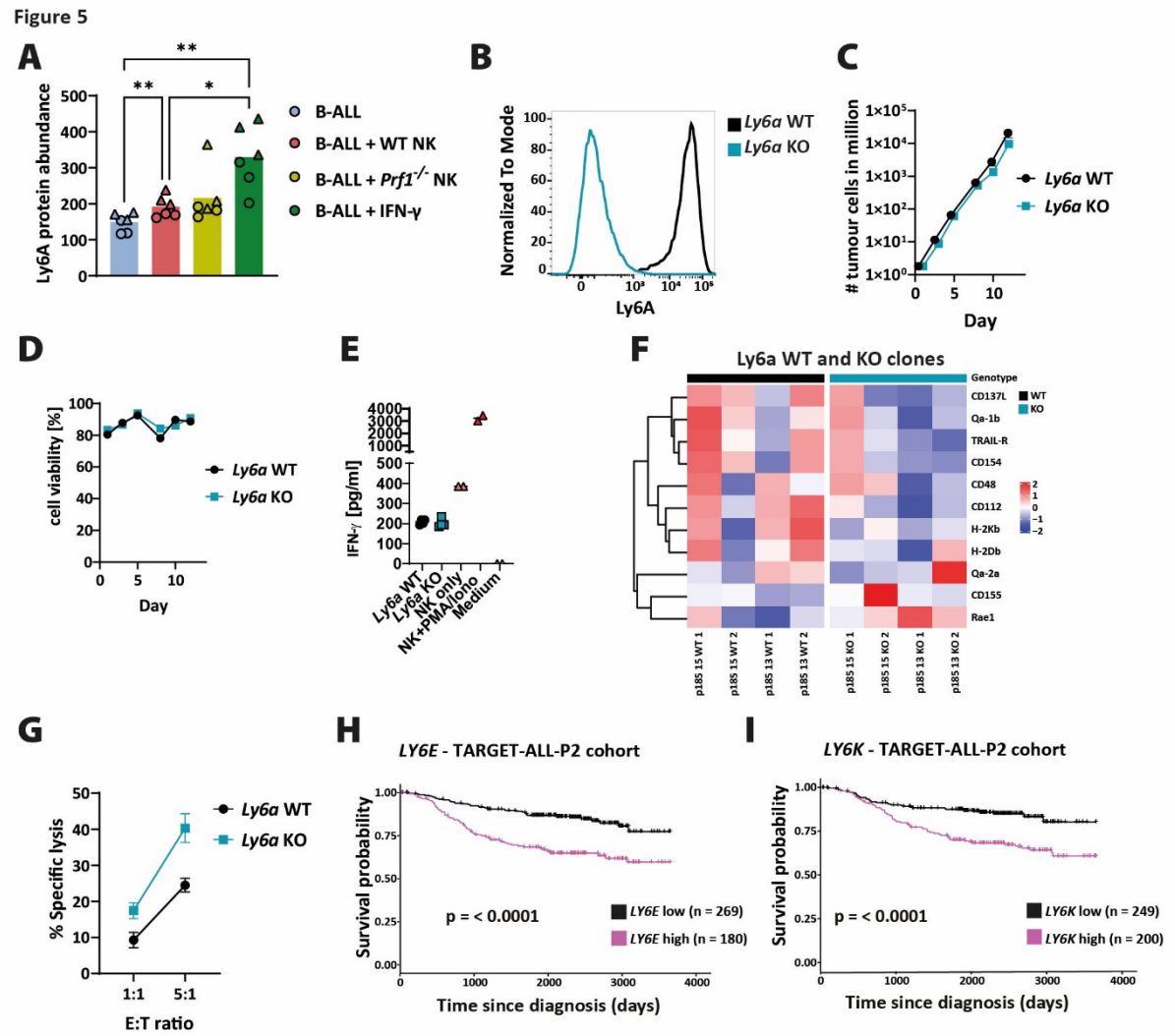

Figure 5: The role of Ly6A in the evasion of leukaemic cells from NK cell-mediated surveillance. (A) Bar graphs show protein abundances of Ly6A on day 14 of the same conditions as in the co-culture experiment described in Figure 4. Two B-ALL cell lines (A in circles/D in triangles) were analysed by mass spectrometry in triplicates. Bars represent means of arbitrary units (AU) relative to the whole protein abundance; the significance was calculated by one-way ANOVA with Tukey post-hoc test. **(B)** *Ly6a* KO clones were generated by ribonucleoprotein transfection into parental B-ALL cell lines. The gene modification was verified by TIDE (Tracking of Indels by Decomposition) PCR and sequencing (not shown) as well as by measuring Ly6A surface expression by flow cytometry. **(C)** Growth curve of *Ly6a* WT and KO B-ALL clones (n=2 per genotype) in absolute cell numbers over 13 days. **(D)** Cell viability of *Ly6a* WT and KO clones (n=2 per genotype) over 13 days. **(E)** Measurement of IFN-γ secretion by mNK cells upon culturing in tumour cell-conditioned medium for 48 h. As positive control mNK cells were

658 activated with PMA/Ionomycin (n=2 clones per genotype and all conditions were in technical
659 duplicates). **(F)** *Ly6a* WT and KO B-ALL cell lines (n=4 per genotype) were characterised by their surface
660 expression of NK ligands by flow cytometry. Columns represent different tumour cell clones ordered
661 according to genotype and cell line. Data has been both scaled and clustered by row to highlight
662 variations in marker expression across different samples. Red indicates higher and blue lower
663 expression levels of surface ligands. **(G)** A 4h standard NK cytotoxicity assay was performed using WT
664 and *Ly6a* KO B-ALL clones. The graph shows the summary data of three independent experiments.
665 Shown are means±SEM of n=2 *Ly6a* WT and KO clones (p-value = 1.15e-8). The p-value was calculated
666 utilising a t-test after fitting the specific lysis values of the 3 biological replicates on a linear model
667 (more details in the methods section). **(H&I)** Kaplan-Meier plots depicting survival probabilities of the
668 TARGET-ALL-P2 patient cohort divided into ***(H)*** *LY6E* and **(I)** *LY6K* high and low expressing groups (cut-
669 off percentile = 60% and 20%, respectively). Graph was generated by using the online web tool:
670 cSurvival (ubc.ca).

671 # Methods

672 ## Mice

673 C57BL/6JRj wild-type mice were obtained from the Janvier labs and C57BL/6-Prf1^{tm1Sdz}/J (*Prf1*$^{-/-}$) mice[26]
674 were obtained from the Jackson Laboratory (Strain #002407). B6.129-B2m^{tm1Jae} (*B2m*$^{-/-}$)[71] mice were
675 kindly provided by Thomas Kolbe (VetMedUni Vienna). The mice were between 8 and 12 weeks of age
676 and maintained under specific pathogen-free conditions according to FELASA guidelines.

677 ## Cell culture

678 To generate BCR/ABL^{p185+} (B-ALL) cell lines, bone marrow was isolated from 8-10-week-old mice and
679 single cell suspensions were prepared through repeated homogenisation using 18G and 24G needles.
680 48 hours before the infection of bone marrow cells, Phoenix-ECO cells (ATCC) were transiently
681 transfected with a retroviral MSCV-BCR/ABL^{p185} vector (kindly provided by Veronika Sexl) mixed with
682 PureFection transfection reagent (System Biosciences). The bone marrow cells were transduced for 1
683 hour with the fresh viral supernatant in the presence of 10 µg/ml polybrene (Sigma Aldrich) and 10
684 ng/ml recombinant murine IL-7 (Peprotech). Transformed B-ALL cell lines were maintained in RPMI
685 medium (Thermo Fisher Scientific) supplemented with 100 U/ml penicillin and 100 µg/ml streptomycin
686 (Thermo Fisher Scientific), 10% fetal bovine serum (FBS) (Capricorn) and 50 µM β-mercaptoethanol
687 (Sigma-Aldrich) (cRPMI).
688 Primary mouse NK cells were isolated from spleens of 8-12-week-old wild-type or *Prf1*$^{-/-}$ mice using the
689 negative selection EasySep mouse NK cell isolation kit (STEMCELL Technologies) or positive selection
690 CD49b (DX5) MicroBeads kit (Miltenyi Biotec) and cultured in cRPMI supplemented with 5,000 U/ml
691 recombinant human IL-2 (Miltenyi Biotec). Mouse NK (mNK) cell purity was measured by flow
692 cytometry with the fixable viability dye eFluor 780 (Invitrogen) and the following antibodies purchased
693 from Miltenyi Biotec: mCD335 (REA815), mCD45.2 (REA1223), mNK1.1 (REA1162) and mCD3 (REA641).
694 mNK cells were identified by gating on single viable mCD45.2^{+} mCD3^{-} NK1.1^{+} mCD335^{+} cells.
695 Phoenix-ECO and Lenti-X packaging cells (Takara) were cultured in DMEM medium (Thermo Fisher
696 Scientific) with 10% FBS.

697 All cell lines were regularly tested for their mycoplasma negativity by using and following the
698 manufacturer´s instructions of the PCR Mycoplasma detection kit (ABM). Cell growth and survival was
699 measured by regular cell counting using a CASY counter (OLS OMNI Life Science).

700 DNA barcoding

701 **Generation of the lentiviral barcode library LG2.1**

702 The BC1DS_lib oligo containing a 21nt random barcode sequence (**Table S1**) was PCR amplified (14
703 cycles: 10sec 98°C, 30 sec 57°C, 20 sec 72°C) with Phusion polymerase (New England Biolabs (NEB)).
704 The resulting PCR amplified product was column purified (MinElute PCR cleanup kit, Qiagen) and
705 subsequently digested with XhoI and AscI, followed by ligation into the 3' UTR of the GFP cDNA
706 sequence within the pRRL lentiviral vector, using the Electroligase kit (NEB). Electrocompetent
707 ElectroMax Stbl4 bacteria (Invitrogen) were then electroporated with 6 ng ligation product and a small
708 fraction of the transformed bacteria was plated on Luria-Bertani (LB) agar plates to determine
709 transformation efficiency, while the remaining bacteria were grown overnight in 400 ml LB medium
710 (VWR Life Science) supplemented with 100 µg/ml ampicillin (Sigma Aldrich). DNA was extracted from
711 the bacterial culture using the Maxiprep kit (Invitrogen).[17,72] This barcode library was kindly provided
712 by Ton Schumacher and amplified further to generate our in house library. ElectroMax Stbl4 bacteria
713 were transformed with 10 ng barcode library to achieve a transformation rate of 100 times the
714 estimated barcode diversity of the library. Bacteria were cultured on LB agar medium (bacteriological
715 agar, tryptone, yeast extract (Oxoid) and sodium chloride (Roth)) petri dishes with 100 µg/ml ampicillin
716 and on the next day resuspended in 50 ml LB medium (tryptone, yeast extract and sodium chloride)
717 with 100 µg/ml ampicillin. Bacteria were expanded in up to 400 ml liquid culture. DNA was extracted
718 with EndoFree Plasmid Maxi Kit (Qiagen). To determine the library's barcode diversity and distribution,
719 barcodes were amplified with a three PCR reaction protocol (see below) in biological and technical
720 duplicates and sequenced on a HiSeq 3000/4000 device (Illumina) with 64 bp single-end reads at the
721 Biomedical Sequencing Facility (BSF) Vienna.

722 **Barcoding of tumour cells**

723 Lenti-X cells were transfected with the LG2.1 barcode library and the two packaging plasmids p8.9QV
724 (provided by Ton Schumacher) and VSVG (provided by Veronika Sexl) using the PureFection
725 transfection reagent. Virus supernatant was harvested after 48 hours and 72 hours and concentrated
726 with AMICON columns (Sigma Aldrich). $2x10^5$ B-ALL cells were spinfected with serially diluted viral
727 supernatant for 90 minutes at 900xg. The transduction rate (% GFP^+ cells) was measured by flow
728 cytometry 3 days after transduction. Tumour cells with the desired transduction rate (<5%[16]) were
729 expanded and FACS sorted to enrich GFP^+ cells. Barcoded tumour cells were frozen for further
730 experiments.

731 ## Flow cytometry

732 ***In vitro* co-culture system and tumour cell growth analysis**

733 $9x10^5$ barcoded B-ALL cells were co-cultured with mNK cells in a effector-to-target (E:T) ratio of 1:1 in
734 three biological replicates per condition. Depending on NK cell cytotoxicity and tumour cell growth,
735 cells were harvested for FACS sorting and further analyses (described below) on day 4 or 6 and for the
736 second time point on day 14 or 16. On the day of harvesting, $3x10^5$ tumour cells were co-cultured for
737 a second or third time with fresh mNK cells (E:T = 1:1). All conditions were cultured in the presence of
738 2,500 U/ml rhIL-2. Wherever indicated, tumour cells treated with 2 ng/ml mouse IFN-γ (Abcam) every
739 2nd to 3rd day, while splitting or expanding the tumour cells.

740 During the co-culture, tumour cell growth was monitored by flow cytometry on a FACSymphony A5
741 Cell Analyzer device (Becton Dickinson). The following antibodies (clones) were purchased from
742 Miltenyi Biotec: mCD45.2 (REA1223), mNK1.1 (REA1162), mCD3 (REA641) and mCD19 (REA749).
743 Zombie Red (Biolegend) was used as viability dye. The absolute number of B-ALL cells was determined
744 with AccuCheck Counting Beads (Invitrogen). Tumour cells were identified by gating on single live
745 $mCD45.2^+$ $mCD19^+$ GFP^+ cells. NK cells were detected by gating on single live $mCD45.2^+$ $NK1.1^+$ $mCD3^-$
746 cells.

747 **Surface marker analysis of tumour cells**

748 Tumour cells were split to $3x10^5$ cells/ml two days before the experiment and 10^6 cells were used for
749 the staining. The following antibodies (clones) were used: CD48 (REA1238), CD112 (829038), CD137L
750 (REA962), CD154 (REA785), CD155 (REA519), TRAIL-R (CD261) (REA1233), Qa-1b (6A8.6F10.1A6), Qa-
751 2a (REA523), H-2Db (REA1198), H-2Kb (REA619), Rae1 (REA723) and Ly6a/Sca-1 (REA422) purchased
752 from Miltenyi Biotec. Single living cells were gated according to size and granularity in FSC-A, SSC-A
753 and FSC-H plots and cell surface marker expression was quantified by median fluorescence intensity
754 (MFI).

755 **Cytotoxicity assay and effector function assay**

756 Cytotoxicity was measured with a flow cytometry-based assay. $5x10^4$ CellTrace Violet (Invitrogen)
757 stained B-ALL cells were seeded in 96-well round bottom plates and IL-2-activated mNK cells added in
758 different E:T ratios (10:1, 5:1, 1:1) in technical duplicates or triplicates. After 4 hours of incubation at
759 37°C, cells were washed with PBS, stained with fixable viability dye eFluor 780 (Invitrogen) and fixed
760 with fixation buffer (Biolegend). Subsequently, samples were measured with a HTS plate reader on an
761 LSR Fortessa device (Becton Dickinson). Percentage of specific NK cell lysis was calculated as follows:
762 (% dead tumour cells after co-incubation with NK cells - % spontaneous lysis) / (100 % - % spontaneous
763 lysis).

764 Multi-omics approaches

765 10^6 GFP^+ barcoded tumour cells were FACS sorted, washed twice with PBS and snap frozen. DNA and
766 RNA were extracted using the AllPrep DNA/RNA Mini Kit (Qiagen).

767 **DNA barcode sequencing**

768 Library preparation for barcode sequencing was performed in technical duplicates with three nested
769 PCR steps. PCR#1 amplified the barcodes, PCR#2 added the required sequences for the universal
770 Illumina adapters and four random base pairs (bps) (BC1v2DS For) for a more diverse sequencing start.
771 PCR#3 attached the P5 and P7 universal Illumina adapters and with the P7 a sample-specific index
772 sequence (Primer sequences are in **Table S1**). The PCR#3 product fragment size (322 bps) was
773 confirmed on a 2% agarose gel electrophoresis for every sample. The samples were cleaned up with

774 Agencourt AMPure XP beads (Beckman Coulter). Up to 96 equimolar pooled samples spiked with 10-
775 15% PhiX (Illumina) were sequenced with the MiSeq Reagent Kit v3 (Illumina) 64 bp single-end reads
776 with an aimed coverage of 50 to 100 reads/barcode.

777 **Barcode/Cell clone evolution analysis**

778 The R statistics software v4.0.3 was used to analyse barcode abundance and clonal diversity.
779 Unmapped reads were loaded from FASTQ format (function *readDNAStringSet* from package
780 Biostrings v2.58.0[73]) into the R environment. First, we located the barcode sequences by pattern
781 matching (function *vmatchPattern* from package Biostrings v2.58.0) to identify the fixed head
782 ("GAACACTCGAGATCAG") and non-variable ("TGTGGTATGATGT") portions of the reads, which directly
783 enclose the barcodes from left and right, respectively. We then extracted the stretch of sequence in
784 between. Sequences that did not meet the expected length (21 bases) or included uncalled bases ("N")
785 were discarded (mean discarded sequences = 15%, **Table S2**). To define the barcodes of the reference
786 library (**Figure S1C-E**), we selected sequences with a sum of at least 100 reads across samples (n = 4)
787 of the viral library for further analysis. With these we constructed a count matrix indicating the number
788 of reads matching each barcode. Next, the technical replicates were merged by adding up the read
789 counts. For each cell line, only barcodes detected across three B-ALL alone samples at the first time
790 point (TP1) or at the second time point (TP2) with a total sum of at least 9 reads were considered for
791 downstream analysis (**Table S3**). Barcode diversity for each sample was quantified using Shannon
792 diversity as follows $sum(p * log(p), na.rm = TRUE) * -1$, where p is the ratio of the counts of
793 each barcode relative to the total barcode counts. We used DESeq2[74] v1.30.0 to find the subset of
794 differentially abundant barcodes (abs[$\log_2$(fold change]_cutoff) ≥ 1 & padj_cutoff < 0.05) across time
795 point and conditions of interest. Shifted $\log_2$ transformation was used for normalisation (function
796 *normTransform* from package DESeq2 v1.30.). Based on the statistics of differential abundance and
797 variability across samples (here, the variability was calculated as following: $v = log2(max(x +$
798 $1)/min(x + 1))$, where x is a vector of normalised counts across samples) at every time point.
799 Barcodes were assigned to one of five categories: i) primary resistant: differentially abundant (padj <
800 0.05) and increasing ($\log_2$(fold change) ≥ 1; comparing B-ALL + NK vs B-ALL alone); ii) eliminated:

801 differentially abundant (padj < 0.05) and decreasing (log_2(fold change) ≤ -1; comparing B-ALL + NK vs
802 B-ALL alone); iii) static: variability v ≤ 0.5 in B-ALL alone, and v < 1 at TP 2; iv) secondary resistant: low
803 variability in B-ALL alone v ≤ 0.5, high variability in B-ALL + NK TP2 v ≥ 1 and barcode abundance high
804 in only one of the three replicates at TP2; v) others: none of the above. Barcodes were further ordered
805 using hierarchical clustering (function *hclust* from package *stats* v 4.0.3*,* method = "ward.d2").
806 Heatmaps were generated using ComplexHeatmap v2.7.5.1 and bubble plots were generated using
807 ggplot2 v3.3.3.

808 **RNA sequencing**

809 After RNA isolation (see above), samples were treated with DNase I (Thermo Fisher Scientific). Library
810 preparation and sequencing was performed at the Biomedical Sequencing Facility (BSF) of the
811 Research Center for Molecular Medicine (CeMM) of the Austrian Academy of Sciences.

812 RNA-seq libraries were prepared with the QuantSeq 3' mRNA-Seq Library Prep Kit (FWD) for Illumina
813 (Lexogen). Library concentrations were quantified with the Qubit 4.0 Fluorometric Quantitation
814 system (Thermo Fisher Scientific) and the size distribution and RNA integrity number were assessed
815 using the 2100 Bioanalyzer instrument (Agilent). For sequencing, samples were diluted and pooled into
816 NGS libraries in equimolar amounts. Expression profiling libraries were sequenced on HiSeq 3000/4000
817 or Novaseq 6000 instruments (Illumina) following a 50-base-pair and 120-base-pair single-end setup,
818 respectively. Raw data acquisition and base calling was performed on-instrument, while the
819 subsequent raw data processing off the instruments involved two custom programs based on Picard
820 tools (2.19.2). In a first step, base calls were converted into lane-specific, multiplexed, unaligned BAM
821 files suitable for long-term archival (IlluminaBasecallsToMultiplexSam, 2.19.2-CeMM). In a second
822 step, archive BAM files were demultiplexed into sample-specific, unaligned BAM files
823 (IlluminaSamDemux, 2.19.2-CeMM).

824 **RNA-seq analysis**

825 The obtained raw reads were processed using the Snakemake pipeline[75]. Mapping of the reads was
826 performed using STAR[76] (v2.7.10a) to the Genome Reference Consortium Mouse Build 38 (GRCm38),
827 and duplicate reads were identified with Picard (v2.27.4). Quantification of the mapped reads was

828 carried out using Salmon[77] (v1.8.0). The following data processing and visualisation was performed in
829 R (v4.2.0). To ensure robustness of the analysis, the data set was filtered to include only transcripts
830 detected in at least three samples. The analysis of cell lines A and B (both established from cell line
831 #13) was performed separately from the analysis of cell line C and D (both originating from cell line
832 #15). Finally, the results were compared.
833 For count normalisation, variance stabilization, and differential expression analysis, the Bioconductor
834 DESeq2[74] (1.38.3) package was used. DESeq2 employs a negative binomial distribution-based model,
835 with additional shrinkage using apeglm[78] algorithm (v1.20.0). Transcripts were considered significantly
836 differentially expressed between groups of comparison if they exhibited a $\log_2$(fold change) ≥ 0.58 and
837 a padj ≤ 0.05. Only these transcripts were selected for subsequent analysis steps.
838 The initial exploratory analysis included principal component analysis (PCA), production of expression
839 heatmaps and volcano plots using ggplot2 (v3.4.2) and heatmap (v1.0.12). To correct for batch effects
840 between different experiments in PCA plots (**Figures S3A&B, S4A**) the limma R[79] package (v3.54.2) was
841 utilised. The resulting gene lists were annotated and subjected to gene set enrichment analysis (GSEA).
842 Visualisation of the GSEA results was achieved using the hypeR[68] package (v2.0.1) and represented as
843 dot plot. Gene Ontology Biological Process (GOBP) terms were obtained from the Molecular Signatures
844 Database (MSigDB) using the msigdbr[80] (v7.5.1) package.
845 **ATAC sequencing**
846 $5x10^4$ GFP^+ tumour cells were FACS sorted into 1.5 ml micro centrifuge tubes containing 400 µl PBS
847 (Sigma Aldrich) and 0.5% Bovine Serum Albumin (BSA, GE Healthcare) and pelleted. Cell lysis and DNA
848 tagmentation was performed in a total volume of 25 µl of 2x TD (Tagment DNA Buffer) and TDE1
849 (Tagment DNA enzyme) (Illumina), 1% Digitonin (Promega) and 50x EDTA-free Protease Inhibitor
850 Cocktail (Roche) for 30 minutes at 37°C. Samples were purified with the Qiagen MinElute kit (Qiagen).
851 Libraries were generated as described by Buenrostro et al[81] by using the Ad1_noMx and Ad2.1-Ad2.48
852 indexed primers (**Table S1**). PCR products were purified with Agencourt AMPure XP beads and sample
853 profile was analysed with the High Sensitivity D5000 kit (Agilent Technologies) on a TapeStation

854 (Agilent Technologies). 45-48 equimolar pooled samples were sequenced on a NovaSeq 6000
855 instrument with 50 bp paired-end reads at the BSF (CeMM).

856 **ATAC-seq analysis**

857 The obtained raw reads were processed using the ATAC-seq Next Flow[82] pipeline (v2.0). This included
858 mapping the reads with STAR to the GRCm38 genome, identification of duplicates with Picard
859 (v2.27.4), calling broad peaks with MACS2[83] (v2.2.7.1). Peaks overlapping with blacklisted (GRCh38)
860 regions were filtered out and the remaining peaks were annotated with HOMER[84] (v 4.11). Consensus
861 peaks across all samples were identified with BEDTools[85] (v2.30.0) and counting reads in these peaks
862 was done with featureCounts[86] (Rsubread v2.0.1). Visualisation of the ATAC-seq peaks was performed
863 by creation of BigWig files with bedGraphToBigWig (v377) and the following export to IGV[87] browser
864 (v2.16.1). Quality of the obtained raw data was assessed with MultiQC[88] (v1.13). The following data
865 processing and visualisation was performed in R (v4.2.0). To ensure robustness of the analysis, the data
866 set was filtered to include only consensus peaks detected in all three replicates of each condition and
867 cell line and only the peaks that were located in the window of ±3kb around transcription start site
868 (TSS). The analysis of cell lines A and B was performed separately from the analysis of cell line C and D.
869 Similar to the RNA-seq analysis, the Bioconductor DESeq2 (1.38.3) package was used for counts
870 normalisation, variance stabilisation, and analysis of differential accessibility. Peaks were considered
871 significantly accessible between groups of comparison if they exhibited a $\log_2$(fold change) ≥ 0.58 and
872 a padj ≤ 0.05. Exploratory analysis included PCA, production of heatmaps, volcano plots and GSEA.

873 **Integration of RNA-seq and ATAC-seq data**

874 To integrate two datasets and perform genome-wide quantification of differential transcription factor
875 activity in cell lines at different time points we used diffTF[69] (v1.8). The processing was done only for
876 A and B data sets, due to very high computational demand of the algorithm. The input consisted of
877 raw ATAC-seq reads in BAM files, filtered consensus peaks from the previous step, raw RNA-seq counts,
878 and PWM data for all TFs – HOCOMOCO[70] (v10).

879 **2D-RP/RP Liquid Chromatography – Tandem Mass Spectrometry analysis**

880 Cells were lysed in 200 µL lysis buffer (50 mM HEPES pH 8.0, 2% SDS, 1 mM PMSF, cOmplete Protease
881 Inhibitor Cocktail, Roche), heated to 99 °C for 5 min, and DNA was sheared using a Covaris S2
882 ultrasonicator. Lysates were cleared at 20,000 × g for 15 min at 20 °C and tryptic digest was performed
883 using FASP according to Wisniewski et al[89]. Peptides were desalted (C18 SPE; Pierce peptide desalting
884 columns, Thermo Fisher Scientific), labelled with TMTpro™ 16plex reagents according to
885 manufacturer´s instructions (Thermo Fisher Scientific), pooled, dried in a vacuum concentrator, and
886 cleaned up via C18 SPE. After re-buffering in 10 mM ammonium formiate buffer pH 10, peptides were
887 fractionated via a C18 column (150 × 2.0 mm Gemini-NX, 3 µm, C18 110Å, Phenomenex, Torrance, CA,
888 USA) on a Dionex UltiMate 3000 nanoLC (Thermo Fisher Scientific). Fractions were dried in a vacuum
889 concentrator and taken up in 0.1% TFA before analysis.
890 Mass spectrometry analysis was performed on an Orbitrap Fusion Lumos Tribrid mass spectrometer
891 (Thermo Fisher Scientific) coupled to a Dionex UltiMate 3000 nanoLC system (Thermo Fisher Scientific)
892 via a Nanospray Flex Ion Source (Thermo Fisher Scientific) interface using the same procedure as Block
893 et al[90]. Data analysis was performed using the Proteome Discoverer v.2.4.1.15 platform.

894 Genome editing

895 **Ribonucleoprotein (RNP)-mediated CRISPR genome editing of B-ALL cells**

896 RNP electroporation: crRNAs, Alt-R CRISPR Cas9 tracrRNA ATTO 550 and Alt-R S.p. Cas9-GFP V3 were
897 purchased by Integrated DNA Technologies (IDT). Cells were transfected according to manufacturer´s
898 instructions using the following electroporation settings: 350 V, 5 ms and 1 pulse with the Gene Pulser
899 Xcell electroporation system (BioRad). crRNA sequences: *Ly6a*: TCACGTTGACCTTAGTACCC;
900 TATTGAAAGTATGGAGATCC, *Plaat3*: CGTCATGTTTGTTATTGACC; ATGGCCCAGTGTCTGTACAT. The next
901 day tumour cells were FACS sorted for GFP and ATTO 550 double positivity. After assessing editing
902 efficiency by TIDE sequencing (described below) of the bulk population, cells were single cell FACS
903 sorted into 96-well flat bottom plates into 50% tumour cell conditioned medium and 50% fresh cRPMI.
904 After the outgrowth of single clones, the KO was validated by TIDE sequencing. Therefore, up to $2x10^5$
905 cells were pelleted and lysed in 50 µl Pawel´s buffer (50 mM potassium chloride (Roth), 10 mM Tris-

906 HCl pH9 (Sigma Aldrich), 0.45% Nonidet-p40 (Calbiochem), 0.45% Tween 20 (Sigma), 0.8 mg/ml
907 proteinase K (Biozym) in deionized water) at 56°C for 15 minutes with subsequent heat inactivation at
908 95°C for 5 minutes. After centrifugation at 2000xg for 5 minutes, supernatant was used for the TIDE
909 PCR to amplify the breakpoints of the guide RNAs (primer sequences in **Table S1**). PCR products were
910 Sanger sequenced (Microsynth) and analysed for their genotype with the TIDE (nki.nl) web tool. Gene
911 knockouts were validated using flow cytometry (described above) or quantitative PCR (described
912 below).

913 **Quantitative PCR**

914 For the validation of the *Plaat3* KO in tumour cells, RNA of $2x10^6$ cells was extracted with the Monarch
915 Total RNA Miniprep Kit with "on column" DNase I treatment (NEB). cDNA was generated by using
916 LunaScript RT SuperMix Kit (NEB) and qPCR was performed with the Luna universal qPCR Master Mix
917 (NEB) (primer sequences in **Table S1**).

918 IFN-γ ELISA

919 Tumour cells were split to $3x10^5$ cells/ml on day 0 and cultivated for 48 hours in cRPMI. On day 2, the
920 supernatant was harvested, filtered through a 45 µm filter, and transferred onto IL-2 expanded mNK
921 cells in the presence of 2,500 U/ml IL-2. After 48 hours, mNK cells were harvested and the supernatant
922 was frozen at -80°C. As positive control served the stimulation of mNK cells with PMA/Ionomycin
923 (Invitrogen) 4 hours before the supernatant harvesting. The ELISA was performed according to
924 manufactures protocol (Abcam) and analysed using the analysis tool:
925 "https://www.arigobio.com/elisa-analysis".

926 Statistical analysis

927 Statistical analysis was performed using GraphPad Prism version 8.4.3 for Windows (GraphPad
928 Software; http://www.graphpad.com) using two-tailed unpaired t-tests, one-way, two-way ANOVA or
929 Kruskal-Wallis test as indicated. Where ANOVA showed a statistical difference, Tukey's multiple
930 comparison testing or Dunnett's post-hoc testing was applied. The α level for all tests was set to 0.05,

931 and p values were two tailed. The significance level is indicated as following: *p < 0.05; **p < 0.01;
932 ***p < 0.001; ****p < 0.0001).
933 To pool the data from independent cytotoxicity assays (n=3 experiments, Figures 5C&F), a linear model
934 with the categorical variables 'Experiment', 'E:T Ratio', 'Genotype', 'Cell line' and 'Replicate' as
935 predictors for the cytotoxicity response was fit using the R function 'lm' which performs a t-test to
936 determine significance of the relationship between the predictor variables and the response variable.
937 For visualisation purposes, the effect of experimental batch on the cytotoxicity response was corrected
938 for by subtracting the estimated linear model coefficients for experiments 2 and 3 from the observed
939 specific lysis values of the respective experiments, as the approach used in the 'removeBatchEffect'
940 function from the R package limma.
941 To generate the heatmap in Figure 1B, the data was pooled from two independent experiments by
942 calculating the mean surface marker expression or mean % specific lysis at E:T=10:1. The values were
943 standardised for each variable (row) using the following calculation: Z-score = (mean of observed
944 values – mean of the samples) / (standard deviation of the samples).
945 Heatmaps in Figure S6D&H were generated by using the R package ComplexHeatmap (version 2.10.0).
946 The raw median fluorescence intensity (MFI) values minus the MFI of their unstained control served
947 as input. Rows (surface markers) were scaled and clustered (unsupervised). Columns (cell lines) were
948 ordered by genotype and cell line.

949 ## Data and code availability

950 The data and codes generated in the current study are available at Github
951 (https://github.com/TumorImmunoEditingLab). All other relevant data are available from the
952 corresponding author.
953

954 ## Acknowledgements

955 We thank Veronika Sexl from the University of Veterinary Medicine Vienna (VetMedUni Vienna,
956 Austria) for providing the BCR/ABL^{p185} construct and Thomas Kolbe (VetMedUni Vienna, Austria) for
957 providing the *B2m*$^{-/-}$ mice. We are grateful to Marcus Tötzl and Anastasiya Hladik for their assistance
958 with ATAC-seq library preparation and mouse experiments, respectively. We thank the CCRI FACS and
959 Bioinformatics Core Units for assistance with cell sorting and bioinformatics/statistics, respectively,
960 the Core Facility Laboratory Animal Breeding and Husbandry of the Medical University of Vienna
961 (MUW, Austria) for taking care of our mice and the Biomedical Sequencing Facility and the Proteomics
962 Facility of the CeMM Research Centre for Molecular Medicine of the Austrian Academy of Sciences for
963 their support on next-generation sequencing and mass spectrometry analysis, respectively. This work
964 was supported by the St. Anna Children's Cancer Research Institute (Vienna, Austria), a DOC fellowship
965 of the Austrian Academy of Sciences awarded to M.C.B. (#25905), and grants from the Austrian Science
966 Fund (10.55776/P32001-B, 10.55776/P34832 and 10.55776/WKP132-B) and the Fellinger
967 Krebsforschung to E.M.P. F.H. is supported by funding from the Alex's Lemonade Stand Foundation for
968 Childhood Cancer (20-17258), and the Austrian Science Fund (10.55776/TAI 454, 10.55776/TAI 732).

969

970 ## Author contributions

971 Conceptualization: E.M.P.

972 Methodology: M.C.B., B.K., E.M.P., with input from J.U., J.C., L.P., T.S., D.G.,

973 Formal analysis: M.C.B., M.R.S, A.B., P.R., E.M.P.

974 Investigation: M.C.B., H.B., A.D., F.O.D., B.K., F.H.-G., L.S., S.S., D.E., D.G.

975 Writing (original draft): M.C.B., E.M.P.

976 Visualization: M.C.B., M.R.S., A.B., E.M.P.

977 Resources: J.U., J.C., M.L., L.P., T.S., F.H., E.M.P.

978 Supervision: F.H., E.M.P.

Funding acquisition: M.C.B., E.M.P.

All authors reviewed and edited the manuscript.

Competing interest declaration

The authors declare no competing interests.

Additional information

Corresponding author: Eva Maria Putz, Center for Physiology and Pharmacology, Institute of Pharmacology, Medical University of Vienna, Waehringerstrasse 13A, 1090 Vienna, Austria. E-mail: eva-maria.putz@meduniwien.ac.at

987 # Supplementary data figures

Supplementary Figure 1

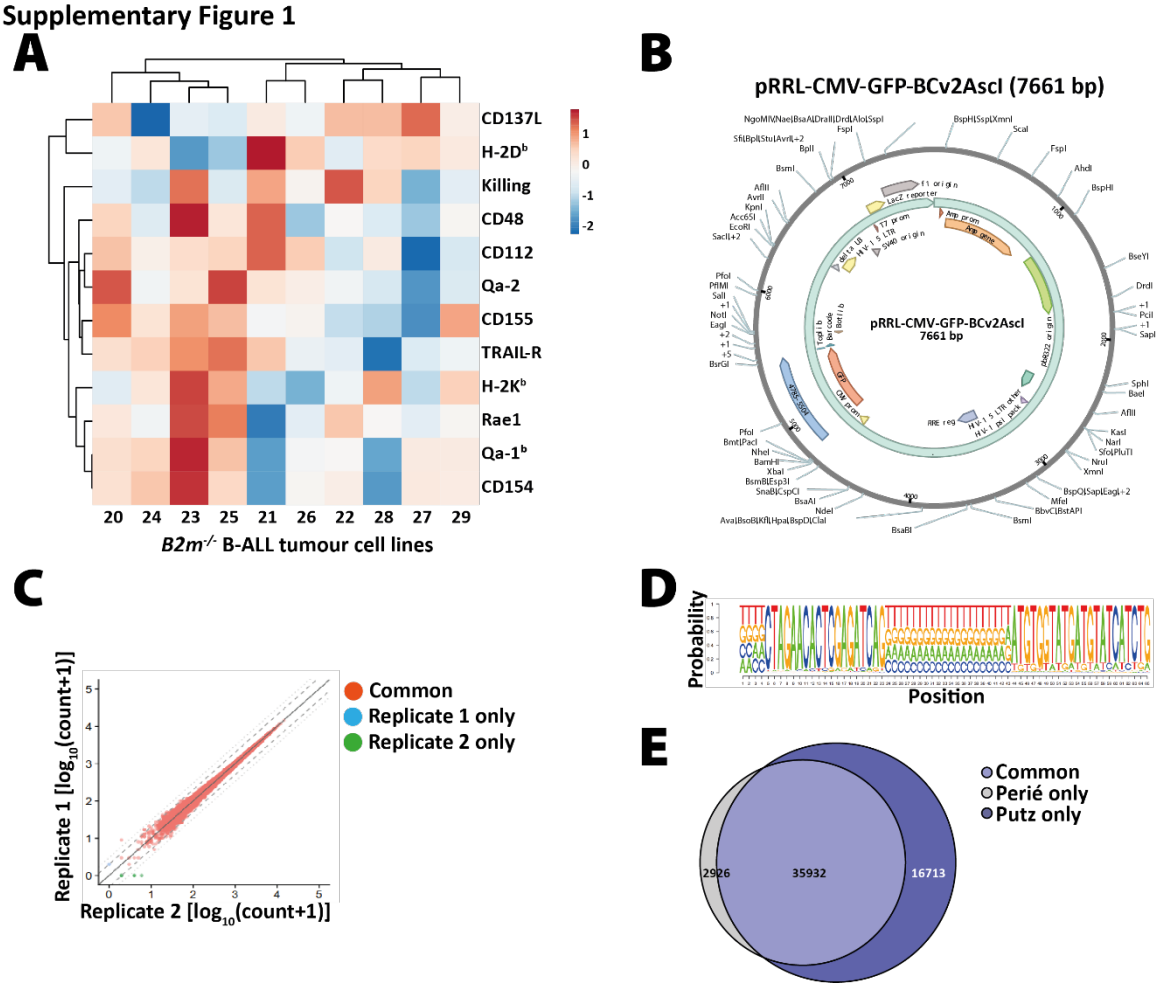

988

989 **Supplementary Figure 1: *B2m*$^{-/-}$ B-ALL cell line characterisation and details about the barcode library.**

990 **(A)** Ten *B2m*$^{-/-}$ B-ALL cell lines were generated from B6.129-B2m^{tm1Jae} (*B2m*$^{-/-}$) mice and characterised

991 regarding the surface expression of NK cell ligands and their susceptibility towards NK cell killing

992 (depicted here is the cytotoxicity at E:T=10:1). Rows were centred; unit variance scaling was applied to

993 rows. Both rows and columns were clustered using correlation distance and average linkage. The plot

994 was generated using the Clustvis web tool[67]. **(B)** Plasmid vector map of the pRRL-CMV-*GFP*-BCv2AscI

995 barcode library plasmid. In the inner circle the CMV promoter, the *GFP* gene, barcode nucleotides

996 (n=21) with Toplib and Botlib primers and the ampicillin resistance are highlighted. Restriction enzyme

997 sites are depicted on the outer circle. **(C)** The barcode library was deep sequenced in technical

998 replicates after plasmid transformation, MaxiPrep and following a 3-step nested PCR library

999 preparation protocol. After raw data processing and filtration for valid barcodes, the barcodes of the

1000 technical replicates were compared and overlapped well. Common barcodes are shown in orange;
1001 non-overlapping barcodes from replicates 1 or 2 are show in blue or green, respectively. **(D)** The graph
1002 shows a representative sequence of one replicate of the barcode library (n=4). Positions 1-4 represent
1003 the random nucleotide insertion after using the BC1v2DS_For primer in PCR#2. Positions 5-23 and 45-
1004 65 are the constant sequences before and after the barcode, respectively. The 21 nucleotides from
1005 positions 24-44 represent the barcode sequence. **(E)** The barcode reference library generated in-house
1006 (Putz laboratory) was compared to the one used in the Périe laboratory. Both libraries, which were
1007 sequenced independently, were overlapping to a high degree. The Putz library detected more
1008 barcodes, which was likely due to the higher sequencing depth.

Supplementary Figure 2

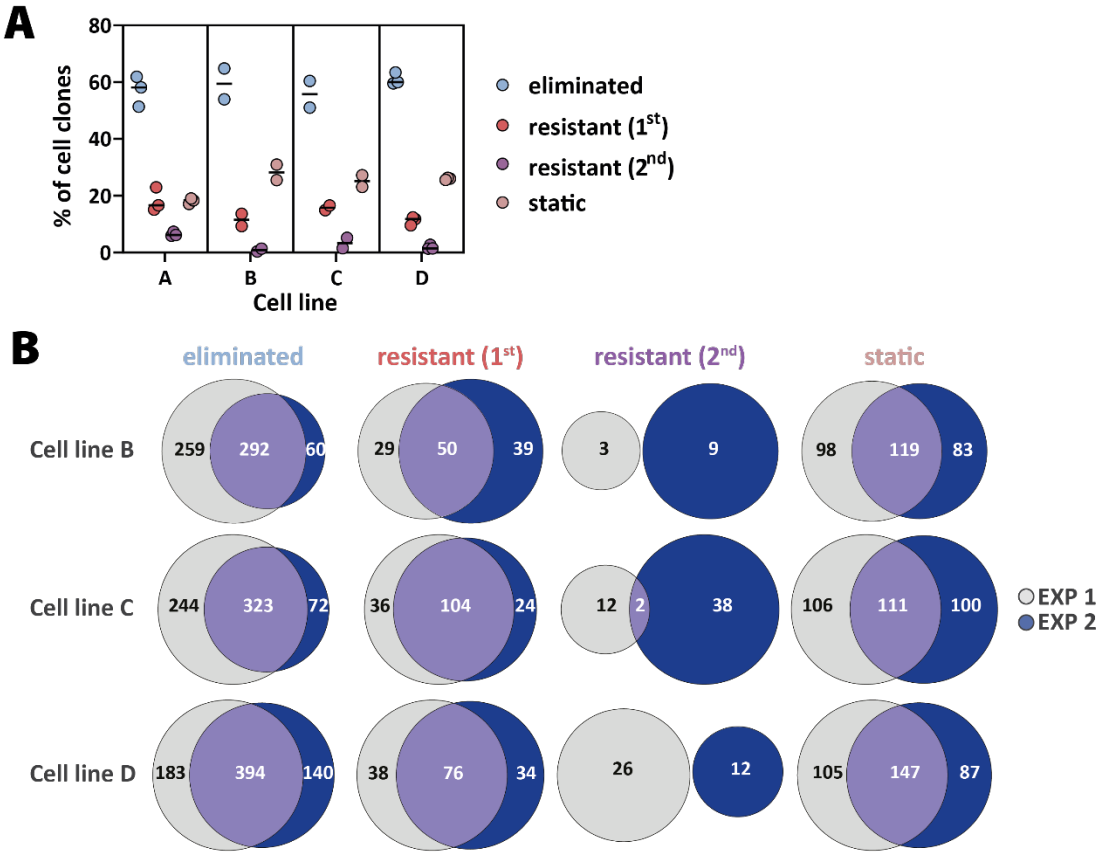

Supplementary Figure 2: Extended quantification of NK cell-mediated cancer immunoediting *in vitro*. According to our hypothesis, the abundance of each barcoded tumour cell clone can be significantly higher (primary resistant) or lower (eliminated), unchanged (static) or show a high variability (secondary resistant) after extended NK cell co-culture. **(A)** The percentage of the cell clones in each group on day 14 is depicted for cell lines A (as shown in Figure 2), B, C and D. Each dot represents the summarised analysis of one independent experiment (plated in three biological replicates and sequenced in technical duplicates). **(B)** Each experiment was performed at least two times using the same barcoded parental cell line. The Euler diagrams compare two individual experiments of cell lines B, C and D (A is shown in Figure 2). The tumour cell clones that were categorised as eliminated, primary resistant, and static showed a relatively high overlap between the two independent experiments. In contrast, secondary resistant clones were less likely to stem from the same original clone when comparing independent experiments.

Supplementary Figure 3

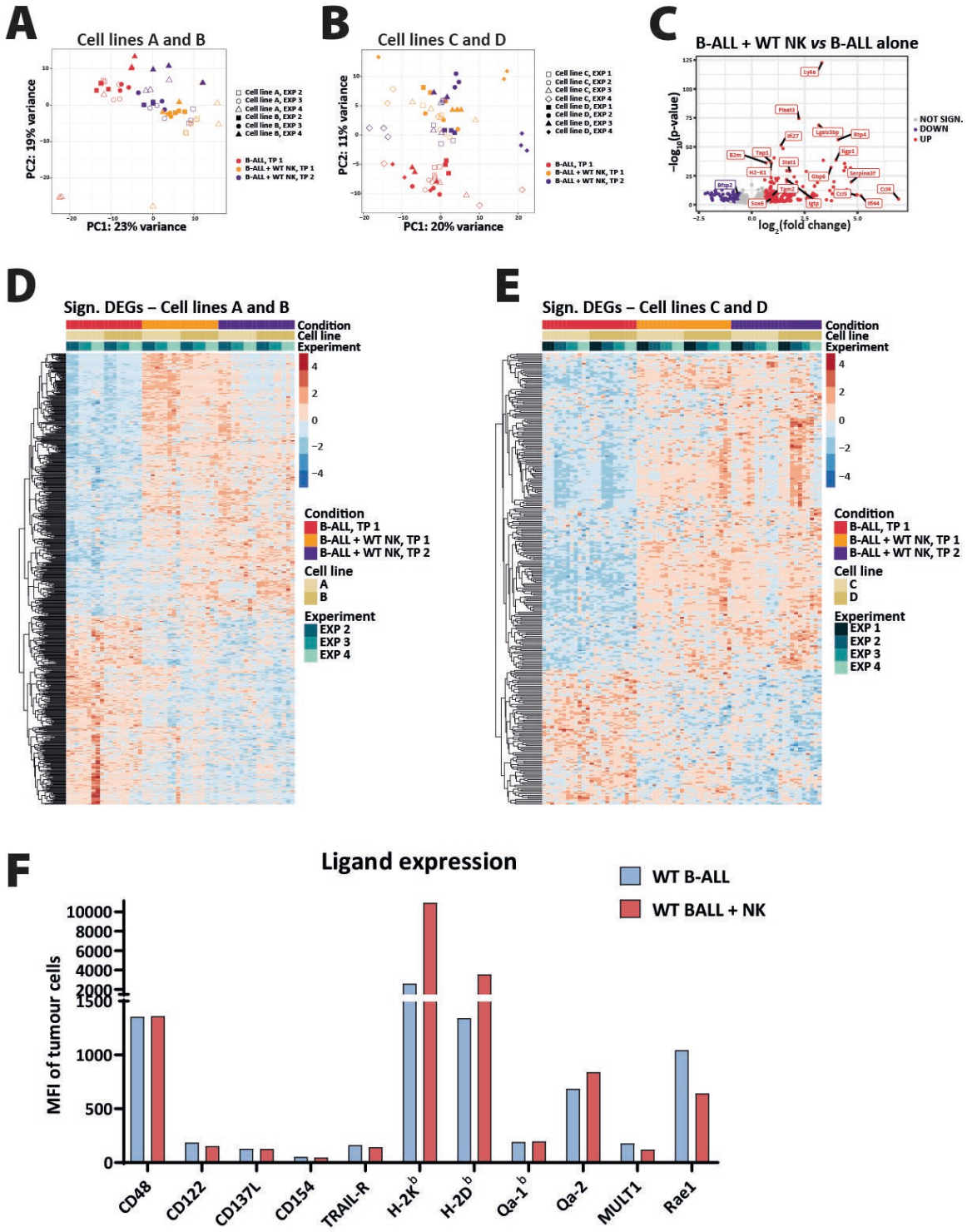

Supplementary Figure 3: Analysis of differentially expressed genes in NK cell resistant tumour cells. **(A&B)** The principal component analysis (PCA) plot illustrates the transcriptomic relatedness among cell lines **(A)** A and B and **(B)** C and D and conditions (B-ALL alone, B-ALL + WT NK cells on time point 1 (TP1) and TP2) in the long-term co-culture experiments, summarising 3 or 4 independent experiments,

1027 respectively. Data was batch corrected for experiments. **(C)** Volcano plot of the RNA-seq analysis of
1028 cell lines C and D showing DEGs of B-ALL + WT NK co-cultured cells (TP2) versus B-ALL alone samples.
1029 **(D&E)** The heat maps summarise DEGs of cell lines **(D)** A and B (n=3 experiments) and **(E)** C and D (n=4
1030 experiments). Heat maps were clustered by condition, cell line and experiment. Z-score $\log_2$(fold
1031 change) is shown and up- or downregulated genes are depicted in red and blue colour, respectively.
1032 **(F)** After 20 days of culturing tumour cell line D with or without NK cells, changes in ligand expression
1033 were measured by flow cytometry. Shown are MFIs gated on the tumour cells.
1034

Supplementary Figure 4

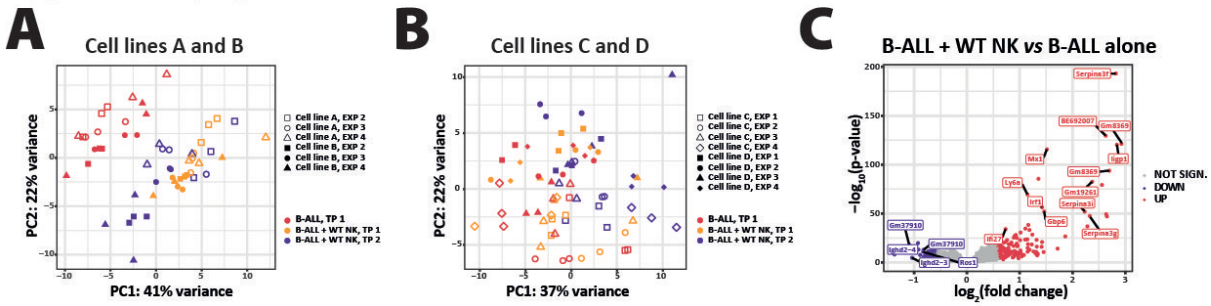

Supplementary Figure 4: Analysis of differentially accessible genes in NK cell resistant tumour cells. (A&B) PCA plots from the ATAC-seq analysis compares the similarities of the chromatin accessibility of the cell lines and the different conditions. Cell lines A and B are shown in **(A)** and C and D in **(B)** summarising 3 and 4 independent experiments, respectively. **(C)** The DARs in B-ALL + WT NK cells at TP2 versus B-ALL alone at TP1 were compared and are shown in a volcano plot summarising 4 independent experiments using cell lines C and D.

Supplementary Figure 5

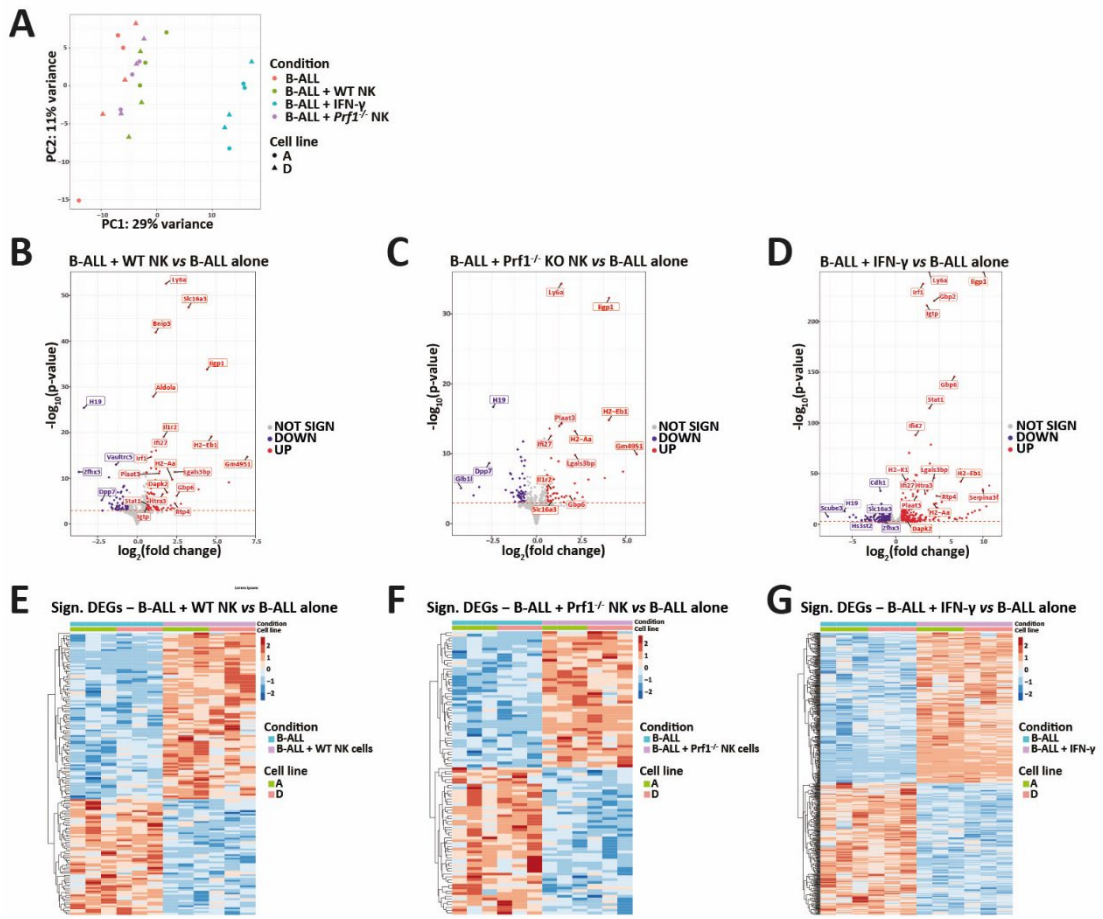

Supplementary Figure 5: Transcriptomic profiles of tumour cells co-cultured with WT NK cells or *Prf1*$^{-/-}$ NK cells or treated with IFN-γ. (A) PCA analysis of the transcriptomic data from RNA-seq shows that the B-ALL cells treated with IFN-γ possess the most unique transcriptome and form a cluster on their own in both cell lines (A and D). Data was batch corrected for experiments. **(B-D)** Volcano plots showing DEGs of the three treatment conditions (B-ALL + WT NK, B-ALL + *Prf1*$^{-/-}$ NK and B-ALL + IFN-γ) compared to the B-ALL alone samples. Analysis includes both cell lines. Differentially up- or downregulated genes are depicted in red and blue, respectively. **(E-G)** Heat maps depicting all up- or downregulated genes of the above-mentioned comparisons. Heat maps were batch-corrected for cell line and clustered by cell line and condition. Z-score $\log_2$(fold change) shows the expression of genes from low to high expression depicted with a colour bar from blue to red.

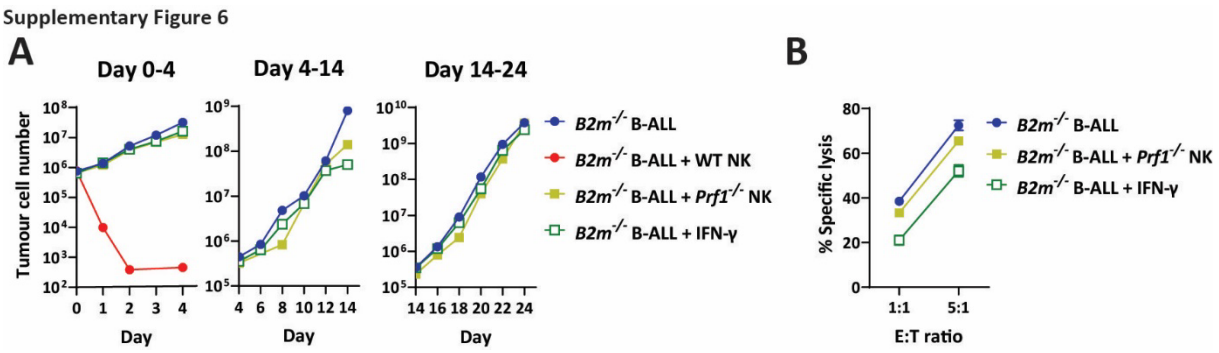

1053

1054 **Supplementary Figure 6: NK cell-derived IFN-γ is a major driver of leukaemia immunoediting. (A)** The
1055 barcoded *B2m*$^{-/-}$ B-ALL cell line was cultivated in three individual wells either in the absence or presence
1056 of purified and IL-2-activated WT or *Prf1*$^{-/-}$ NK cells or with 2 ng/ml IFN-γ. Absolute numbers of B-ALL
1057 cells were determined by flow cytometry. On day 0, 4 and 14 B-ALL cells were FACS sorted, re-plated
1058 and fresh NK cells were replenished. Shown is one representative experiment (n=2 independent
1059 experiments). **(B)** On day 28, a standard 4h NK cytotoxicity assay was performed using *B2m*$^{-/-}$ B-ALL
1060 cells that had been cultured for 27 days in the presence or absence of NK cells or IFN-γ. Shown are
1061 means±SD of one cell line in technical triplicates of one representative experiment (n=2 experiments).

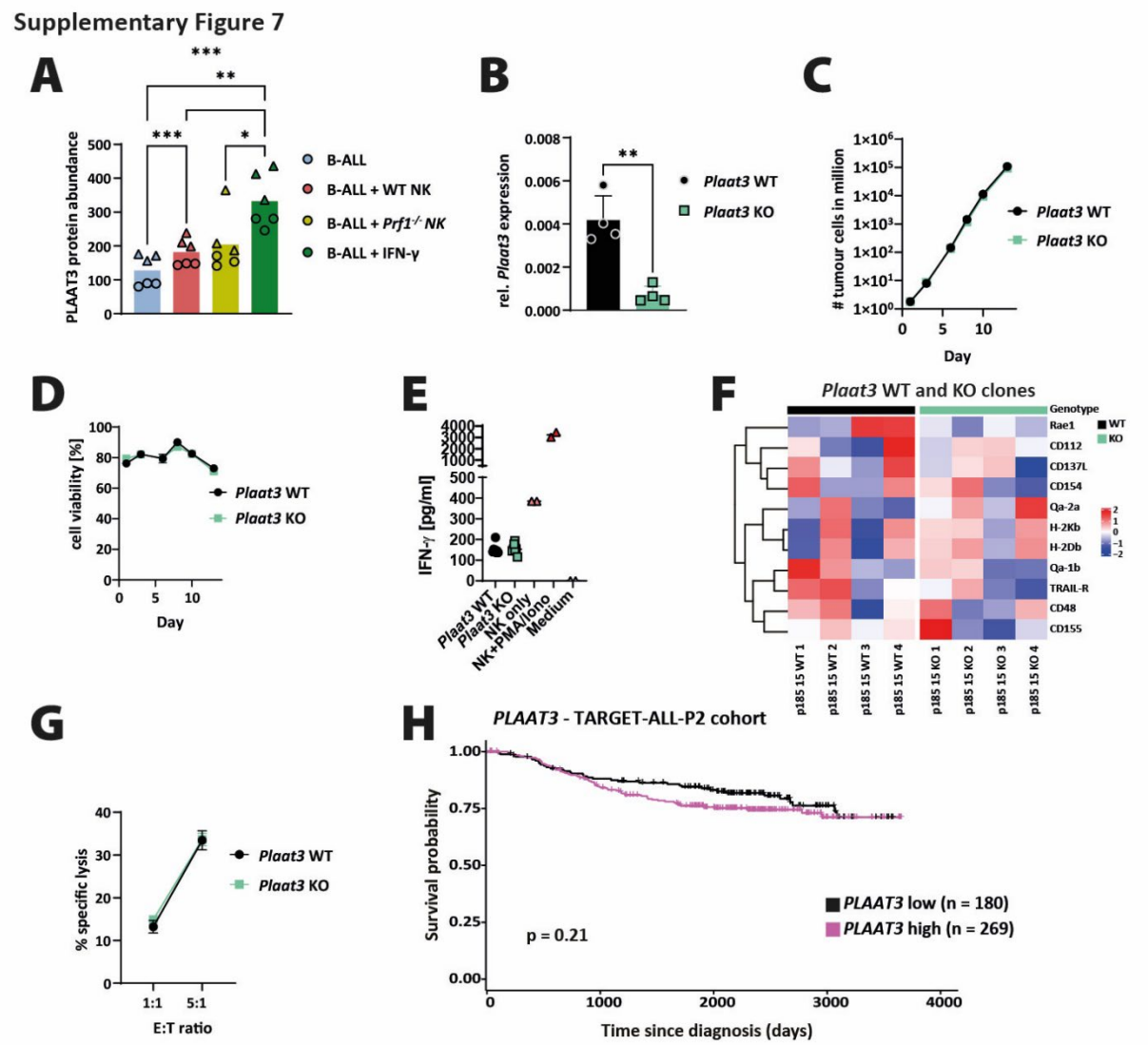

Supplementary Figure 7: Generation of *Plaat3* KO B-ALL clones and their characterisation. (A) Bar graph shows the protein abundance of PLAAT3 on day 14 of the same conditions as in the co-culture experiment described in Figure 4. Two B-ALL cell lines (A in circles/D in triangles) were analysed by mass spectrometry in triplicates. Bars represent means of arbitrary units (AU) relative to the whole protein abundance; the significance was calculated by one-way ANOVA with Tukey post-hoc test. **(B)** *Plaat3* KO clones were generated by ribonucleoprotein transfection into parental B-ALL cell lines. The gene modification was verified by TIDE (Tracking of Indels by Decomposition) PCR and sequencing (not shown) as well as by *Plaat3* mRNA expression analysed by qPCR. Bars and error bars represent means±SD; the significance was calculated using an unpaired t-test. **(C)** Growth curve of *Plaat3* WT and KO clones (n=4 per genotype) showing the proliferation in absolute cell numbers over 13 days. **(D)** Cell viability of *Plaat3* WT and KO clones (n=4 per genotype) measured over 13 days. **(E)** Measurement of

1074 IFN-γ secretion by mNK cells upon culturing in tumour cell conditioned medium for 48 h. As positive
1075 control mNK cells were activated with PMA/Ionomycin (n=4 clones per genotype and all conditions
1076 were in technical duplicates). **(F)** *Plaat3* WT and KO B-ALL cell lines (n=4 per genotype) were
1077 characterised by their surface expression of NK ligands by flow cytometry. Columns represent different
1078 tumour cell clones ordered according to genotype and cell line. Data has been both scaled and
1079 clustered by row to highlight variations in marker expression across different samples. Red indicates
1080 higher and blue lower expression levels of surface ligands. **(G)** A 4h standard NK cytotoxicity assay was
1081 performed using WT and *Plaat3* KO B-ALL clones. The graph shows the summary data of three
1082 independent experiments. Shown are means±SEM of *Plaat3* WT and KO cell clones (n=4 per genotype)
1083 (not significant). The p-value was calculated utilising a t-test after fitting the specific lysis values of the
1084 3 biological replicates on a linear model (more details in the methods section). **(H)** Kaplan-Meier plot
1085 depicting survival probability of the TARGET-ALL-P2 patient cohort divided into *PLAAT3* high and low
1086 expressing groups (cut-off percentile = 40 %). The graph was generated by using the online web tool:
1087 cSurvival (ubc.ca).

1088 ## Supplementary table legends

1089 **Supplementary Table 1: Primers.** Columns show primer name, sequence, usage, annealing
1090 temperature (in °C) and used polymerase.

1091 **Supplementary Table 2: Valid DNA barcode reads.** The table shows the sample name, cell line, invalid
1092 and valid read counts. Invalid reads, which did not match the filter criteria were discarded. Valid read
1093 count divided by total read count indicates the percentage of the retrieved valid reads within a sample.
1094 Listed are EXP 9.6 and EXP 9.7 (Figure 2&S2, n=4 cell lines A-D) and EXP 9.8 (Figure 4&S2A, n=2 cell
1095 lines A and D). All conditions are in triplicates. Example sample name: "Experiment_Cell
1096 line_Condition_Timepoint_Well_Technical replicate".

1097 **Supplementary Table 3: Read counts per barcode of all samples.** The table consists of sheets unique
1098 for each cell line and experiment. Each sheet shows in the rows the barcode sequences (barcode_seq)
1099 detected for the specific cell line and experiment. Columns depict each sample sequenced in technical
1100 duplicates. Shown are EXP 9.6 and EXP 9.7 (Figure 2&S2, n=4 cell lines A-D) and EXP 9.8 (Figure 4&S2A,
1101 n=2 cell lines A and D). All conditions are in triplicates**.** Example sample name: "Experiment_Cell
1102 line_Condition_Timepoint_Well".

1103 **Supplementary Table 4: Antibodies and viability dyes used for flow cytometric analyses.** Indicated
1104 are target antigens, conjugates, clones, suppliers, catalogue numbers and used working dilutions.

Figure 1

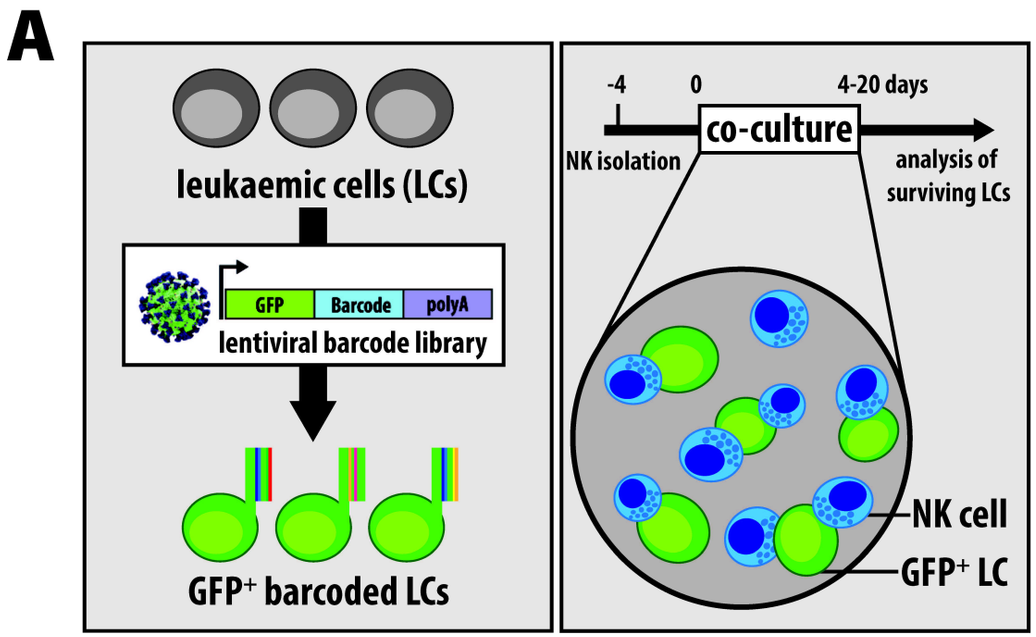
A
leukaemic cells (LCs)
GFP
Barcode
polyA
lentiviral barcode library
GFP+ barcoded LCs
-4
0
4-20 days
co-culture
NK isolation
analysis of surviving LCs
NK cell
GFP+ LC

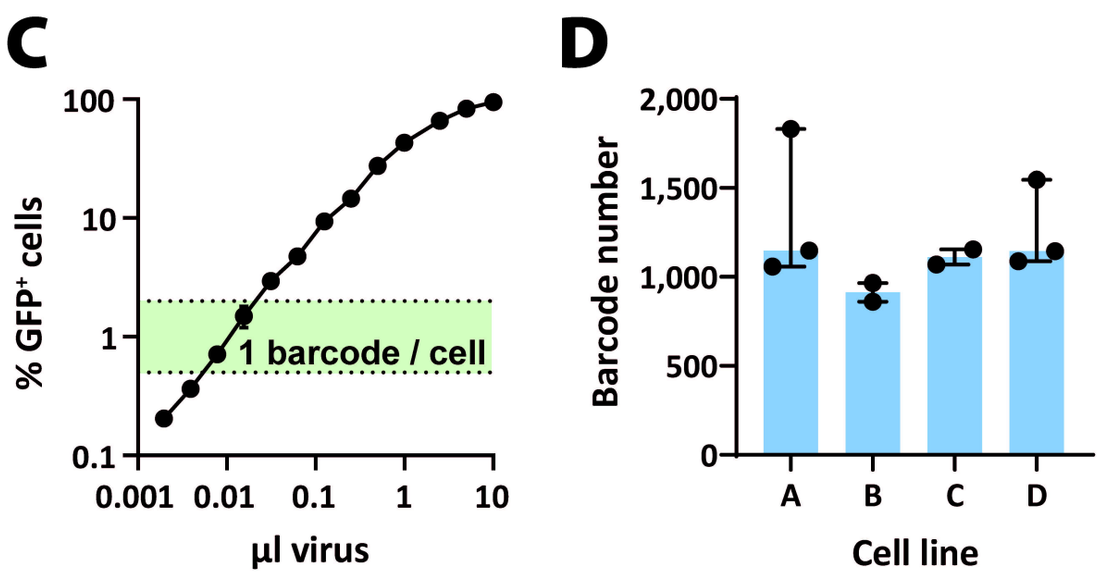
C
% GFP+ cells
100
10
1
0.1
1 barcode / cell
0.001
0.01
0.1
1
10
µl virus
D
Barcode number
2,000
1,500
1,000
500
0
A
B
C
D
Cell line

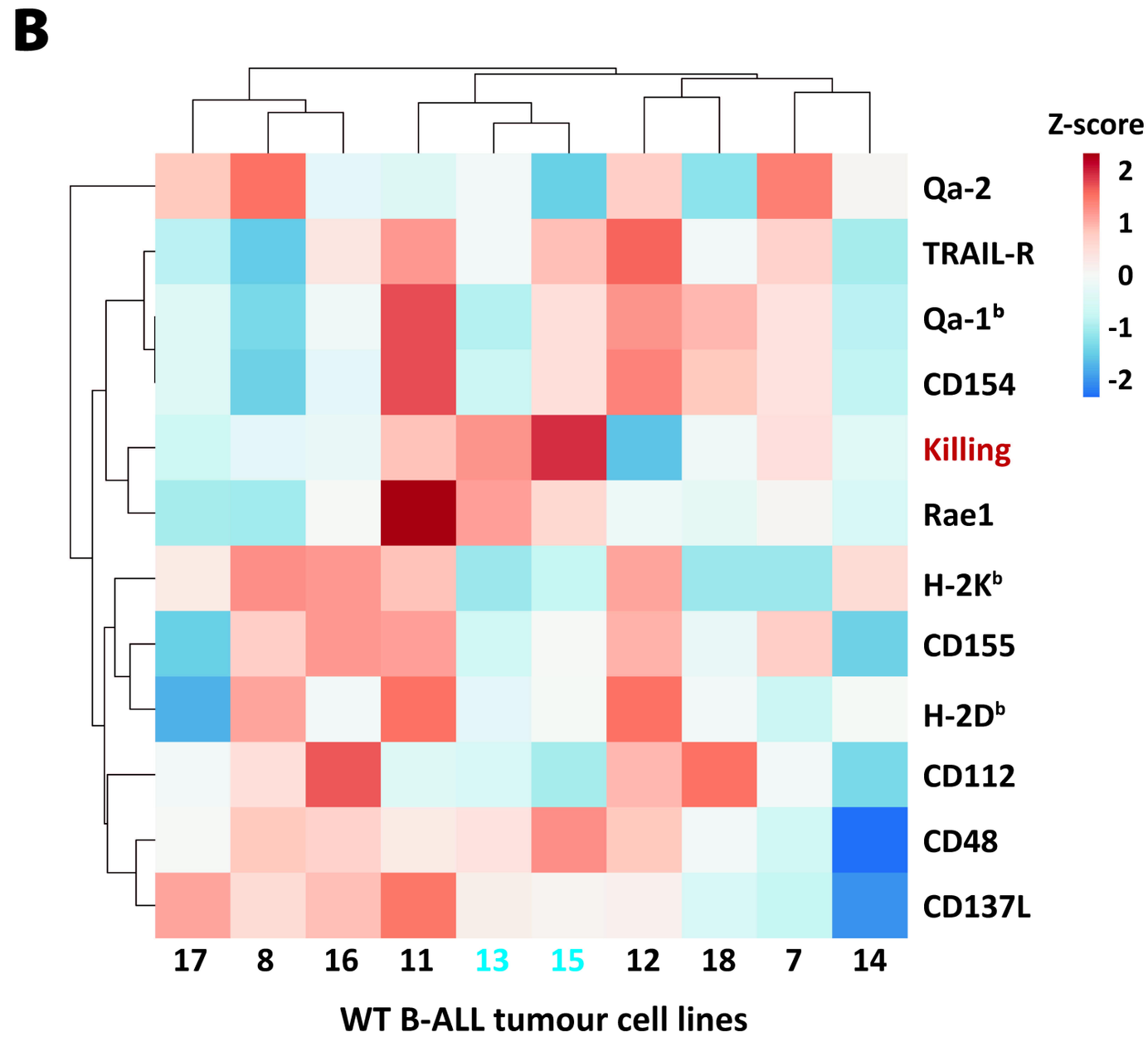
B
Z-score
2
1
0
-1
-2
Qa-2
TRAIL-R
Qa-1b
CD154
Killing
Rae1
H-2Kb
CD155
H-2Db
CD112
CD48
CD137L
17
8
16
11
13
15
12
18
7
14
WT B-ALL tumour cell lines

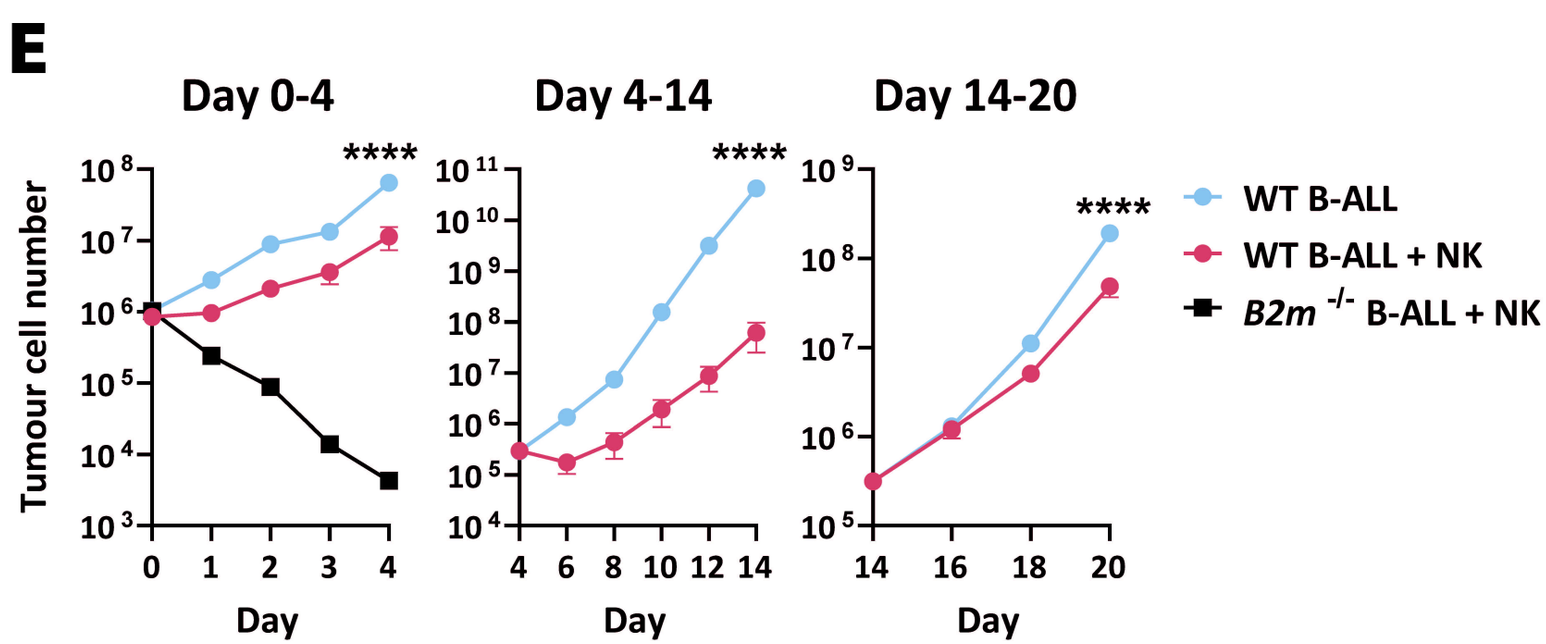
E
Day 0-4
Day 4-14
Day 14-20
Tumour cell number
****
Day
WT B-ALL
WT B-ALL + NK
B2m -/- B-ALL + NK

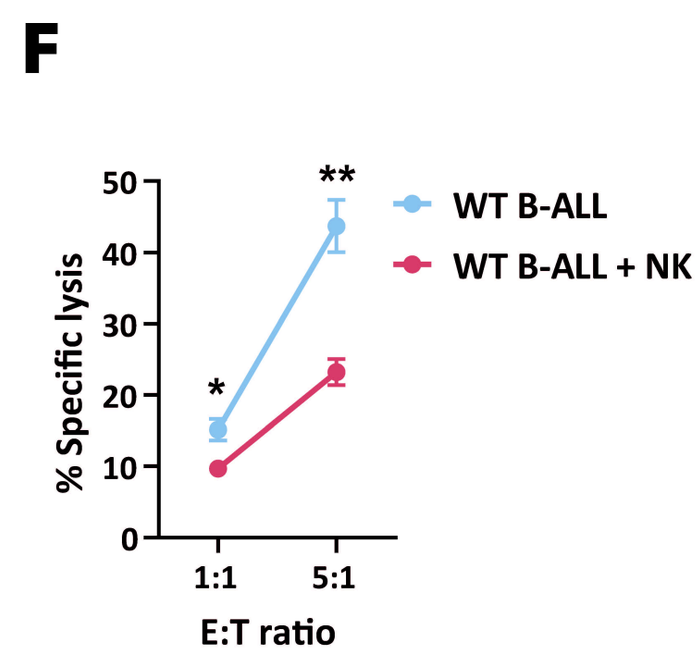
F
% Specific lysis
50
40
30
20
10
0
*
**
1:1
5:1
E:T ratio
WT B-ALL
WT B-ALL + NK

Figure 2

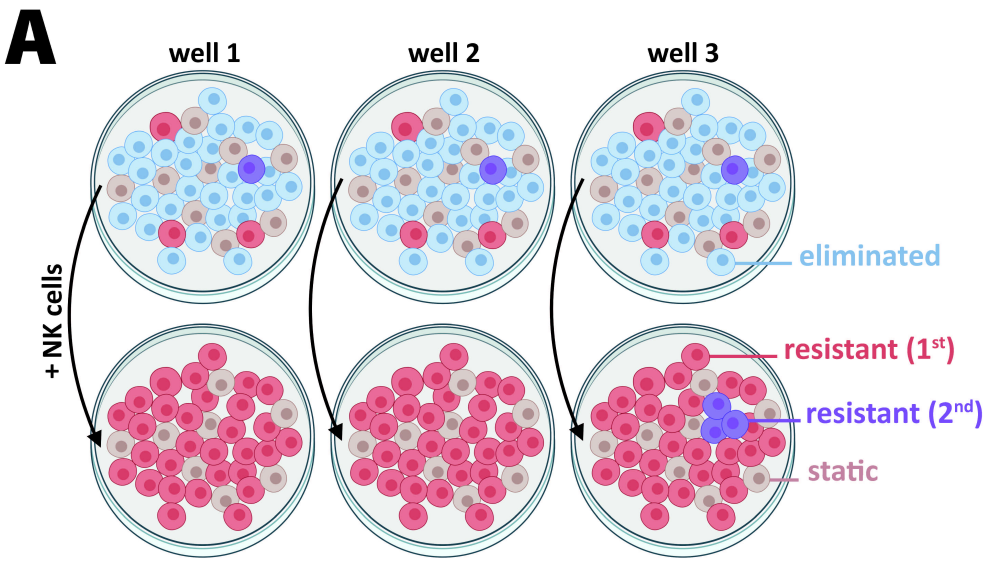
A
well 1
well 2
well 3
+ NK cells
eliminated
resistant (1st)
resistant (2nd)
static

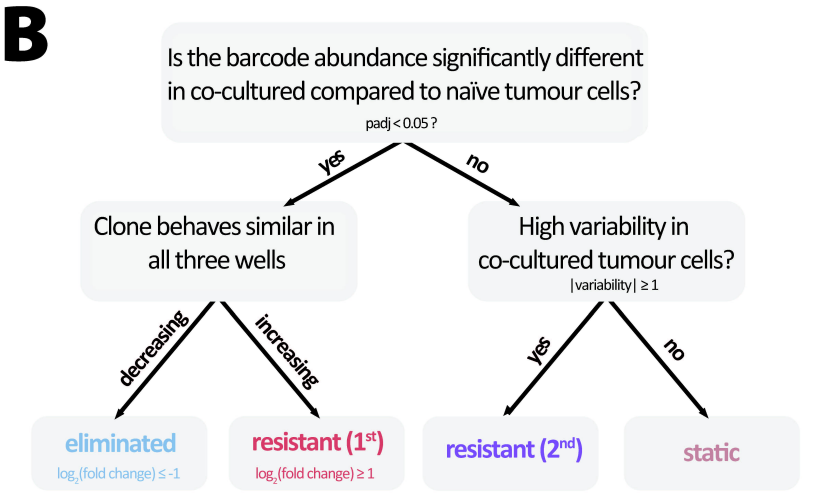
B
Is the barcode abundance significantly different in co-cultured compared to naïve tumour cells?
padj < 0.05 ?
yes
no
Clone behaves similar in all three wells
High variability in co-cultured tumour cells?
|variability| ≥ 1
decreasing
increasing
yes
no
eliminated
log2(fold change) ≤ -1
resistant (1st)
log2(fold change) ≥ 1
resistant (2nd)
static

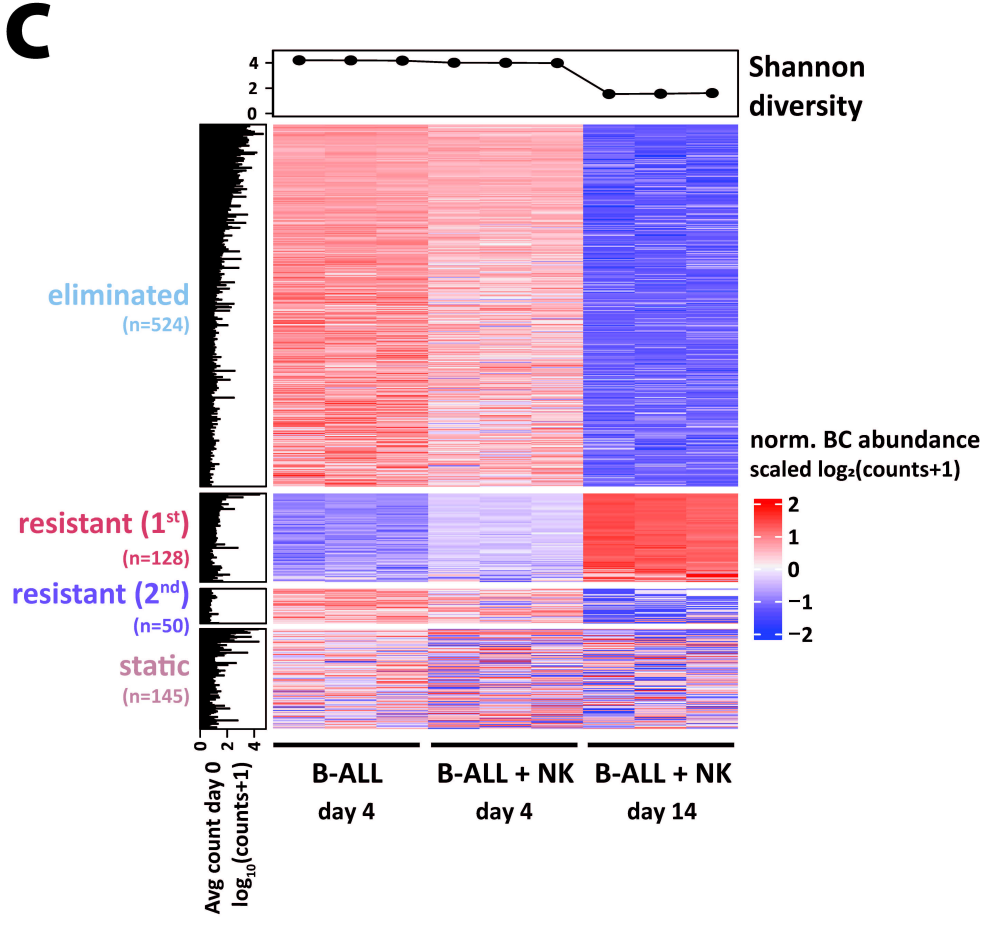
C
Shannon diversity
eliminated
(n=524)
resistant (1st)
(n=128)
resistant (2nd)
(n=50)
static
(n=145)
norm. BC abundance
scaled log2(counts+1)
Avg count day 0
log10(counts+1)
B-ALL
day 4
B-ALL + NK
day 4
B-ALL + NK
day 14

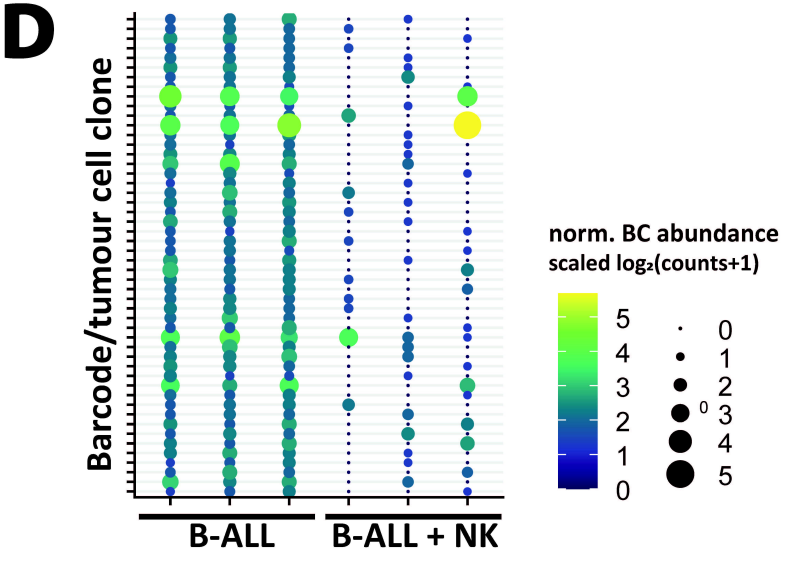
D
Barcode/tumour cell clone
B-ALL
B-ALL + NK
norm. BC abundance
scaled log2(counts+1)

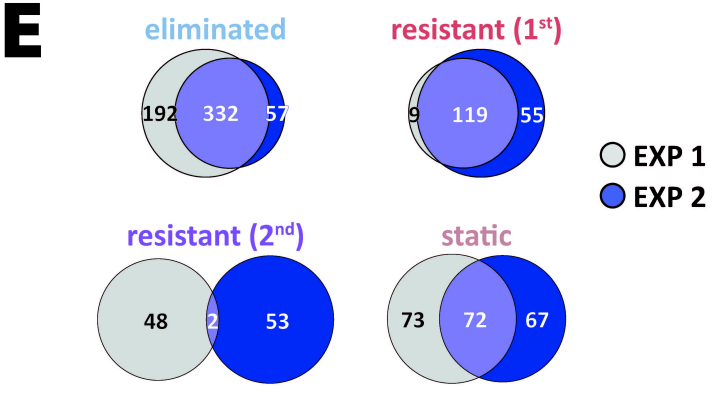
E
eliminated
192
332
57
resistant (1st)
9
119
55
resistant (2nd)
48
2
53
static
73
72
67
EXP 1
EXP 2

Figure 3

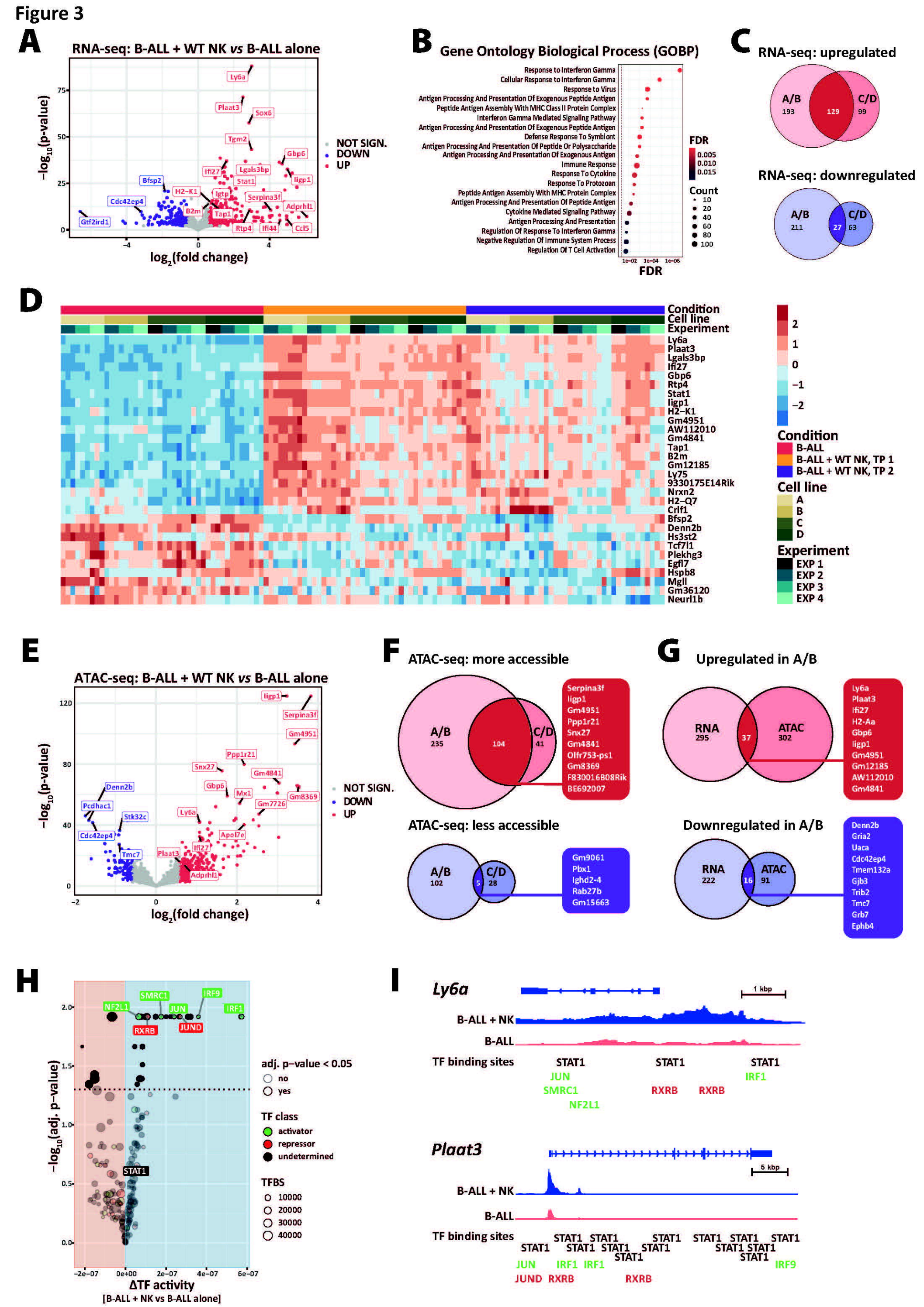
A
RNA-seq: B-ALL + WT NK vs B-ALL alone
−log10(p-value)
log2(fold change)
NOT SIGN.
DOWN
UP
Ly6a
Plaat3
Sox6
Tgm2
Gbp6
Ifi27
Lgals3bp
Stat1
Iigp1
Bfsp2
H2-K1
Igtp
Serpina3f
Adprhl1
Cdc42ep4
B2m
Tap1
Gtf2ird1
Rtp4
Ifi44
Ccl5
B
Gene Ontology Biological Process (GOBP)
Response to Interferon Gamma
Cellular Response to Interferon Gamma
Response to Virus
Antigen Processing And Presentation Of Exogenous Peptide Antigen
Peptide Antigen Assembly With MHC Class II Protein Complex
Interferon Gamma Mediated Signaling Pathway
Antigen Processing And Presentation Of Exogenous Peptide Antigen
Defense Response To Symbiont
Antigen Processing And Presentation Of Peptide Or Polysaccharide
Antigen Processing And Presentation Of Exogenous Antigen
Immune Response
Response To Cytokine
Response To Protozoan
Peptide Antigen Assembly With MHC Protein Complex
Antigen Processing And Presentation Of Peptide Antigen
Cytokine Mediated Signaling Pathway
Antigen Processing And Presentation
Regulation Of Response To Interferon Gamma
Negative Regulation Of Immune System Process
Regulation Of T Cell Activation
FDR
Count
C
RNA-seq: upregulated
A/B 193
129
C/D 99
RNA-seq: downregulated
A/B 211
27
C/D 63
D
Condition
Cell line
Experiment
Ly6a
Plaat3
Lgals3bp
Ifi27
Gbp6
Rtp4
Stat1
Iigp1
H2-K1
Gm4951
AW112010
Gm4841
Tap1
B2m
Gm12185
Ly75
9330175E14Rik
Nrxn2
H2-Q7
Crlf1
Bfsp2
Denn2b
Hs3st2
Tcf7l1
Plekhg3
Egfl7
Hspb8
Mgll
Gm36120
Neurl1b
B-ALL
B-ALL + WT NK, TP 1
B-ALL + WT NK, TP 2
A
B
C
D
EXP 1
EXP 2
EXP 3
EXP 4
E
ATAC-seq: B-ALL + WT NK vs B-ALL alone
−log10(p-value)
log2(fold change)
NOT SIGN.
DOWN
UP
Iigp1
Serpina3f
Gm4951
Ppp1r21
Snx27
Gm4841
Gbp6
Mx1
Gm8369
Gm7726
Denn2b
Pcdhac1
Stk32c
Ly6a
Cdc42ep4
Apol7e
Tmc7
Plaat3
Ifi27
Adprhl1
F
ATAC-seq: more accessible
A/B 235
104
C/D 41
Serpina3f
Iigp1
Gm4951
Ppp1r21
Snx27
Gm4841
Olfr753-ps1
Gm8369
F830016B08Rik
BE692007
ATAC-seq: less accessible
A/B 102
5
C/D 28
Gm9061
Pbx1
Ighd2-4
Rab27b
Gm15663
G
Upregulated in A/B
RNA 295
37
ATAC 302
Ly6a
Plaat3
Ifi27
H2-Aa
Gbp6
Iigp1
Gm4951
Gm12185
AW112010
Gm4841
Downregulated in A/B
RNA 222
16
ATAC 91
Denn2b
Gria2
Uaca
Cdc42ep4
Tmem132a
Gjb3
Trib2
Tmc7
Grb7
Ephb4
H
−log10(adj. p-value)
ΔTF activity
[B-ALL + NK vs B-ALL alone]
NF2L1
SMRC1
JUN
IRF9
IRF1
RXRB
JUND
STAT1
adj. p-value < 0.05
no
yes
TF class
activator
repressor
undetermined
TFBS
10000
20000
30000
40000
I
Ly6a
1 kbp
B-ALL + NK
B-ALL
TF binding sites
STAT1
JUN
SMRC1
NF2L1
RXRB
IRF1
Plaat3
5 kbp
B-ALL + NK
B-ALL
TF binding sites
STAT1
JUN
JUND
IRF1
RXRB
IRF9

Figure 4

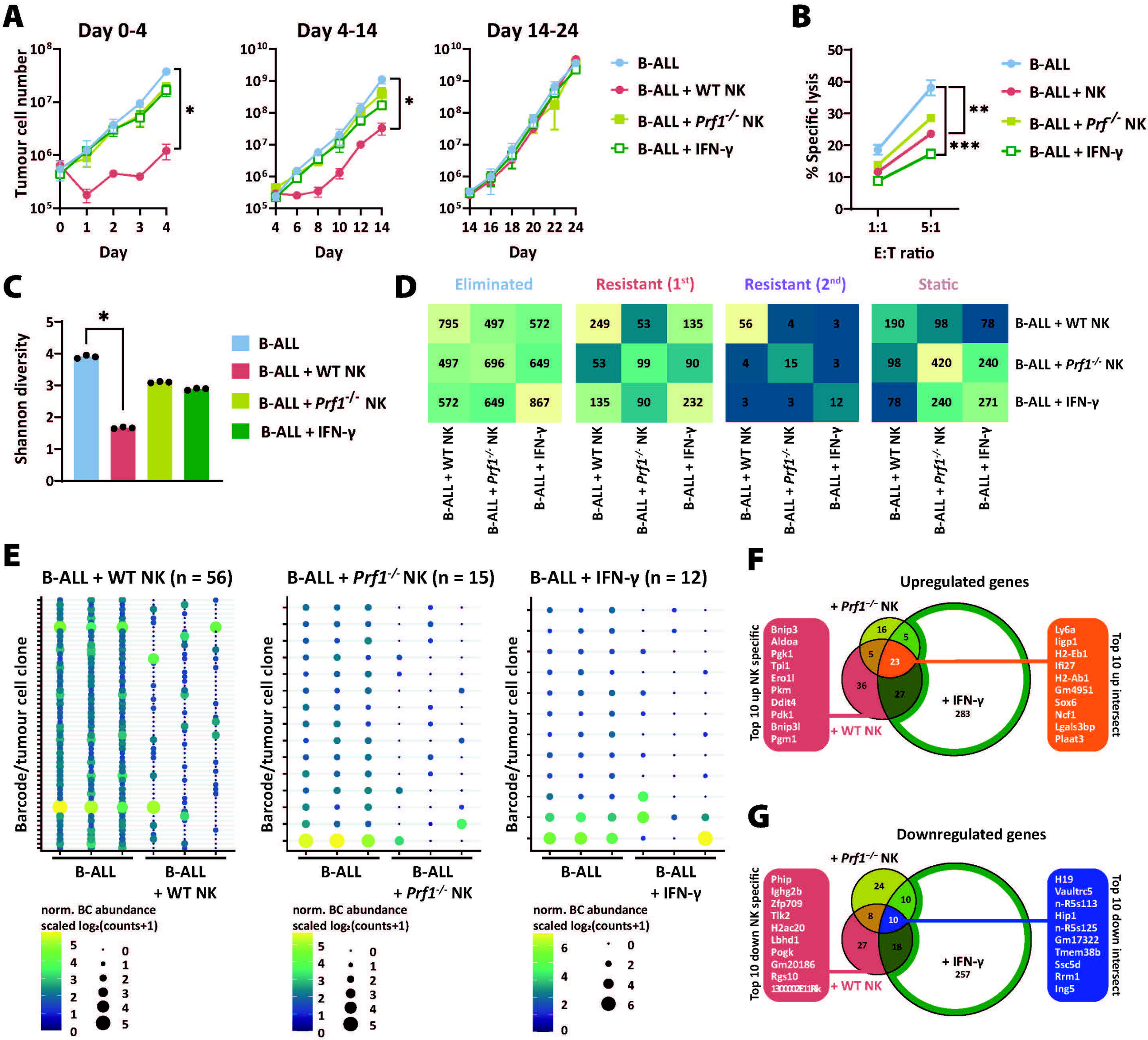
A
Day 0-4
Day 4-14
Day 14-24
Tumour cell number
Day
B-ALL
B-ALL + WT NK
B-ALL + Prf1-/- NK
B-ALL + IFN-γ
B
% Specific lysis
E:T ratio
1:1
5:1
B-ALL + NK
B-ALL + Prf-/- NK
C
Shannon diversity
D
Eliminated
Resistant (1st)
Resistant (2nd)
Static
795 497 572 249 53 135 56 4 3 190 98 78
497 696 649 53 99 90 4 15 3 98 420 240
572 649 867 135 90 232 3 3 12 78 240 271
B-ALL + WT NK
B-ALL + Prf1-/- NK
B-ALL + IFN-γ
E
B-ALL + WT NK (n = 56)
B-ALL + Prf1-/- NK (n = 15)
B-ALL + IFN-γ (n = 12)
Barcode/tumour cell clone
B-ALL
B-ALL + WT NK
B-ALL + Prf1-/- NK
B-ALL + IFN-γ
norm. BC abundance
scaled log2(counts+1)
F
Upregulated genes
+ Prf1-/- NK
+ IFN-γ
+ WT NK
Top 10 up NK specific
Bnip3
Aldoa
Pgk1
Tpi1
Ero1l
Pkm
Ddit4
Pdk1
Bnip3l
Pgm1
Top 10 up intersect
Ly6a
Iigp1
H2-Eb1
Ifi27
H2-Ab1
Gm4951
Sox6
Ncf1
Lgals3bp
Plaat3
G
Downregulated genes
Top 10 down NK specific
Phip
Ighg2b
Zfp709
Tlk2
H2ac20
Lbhd1
Pogk
Gm20186
Rgs10
1300002E11Rik
Top 10 down intersect
H19
Vaultrc5
n-R5s113
Hip1
n-R5s125
Gm17322
Tmem38b
Ssc5d
Rrm1
Ing5

Figure 5

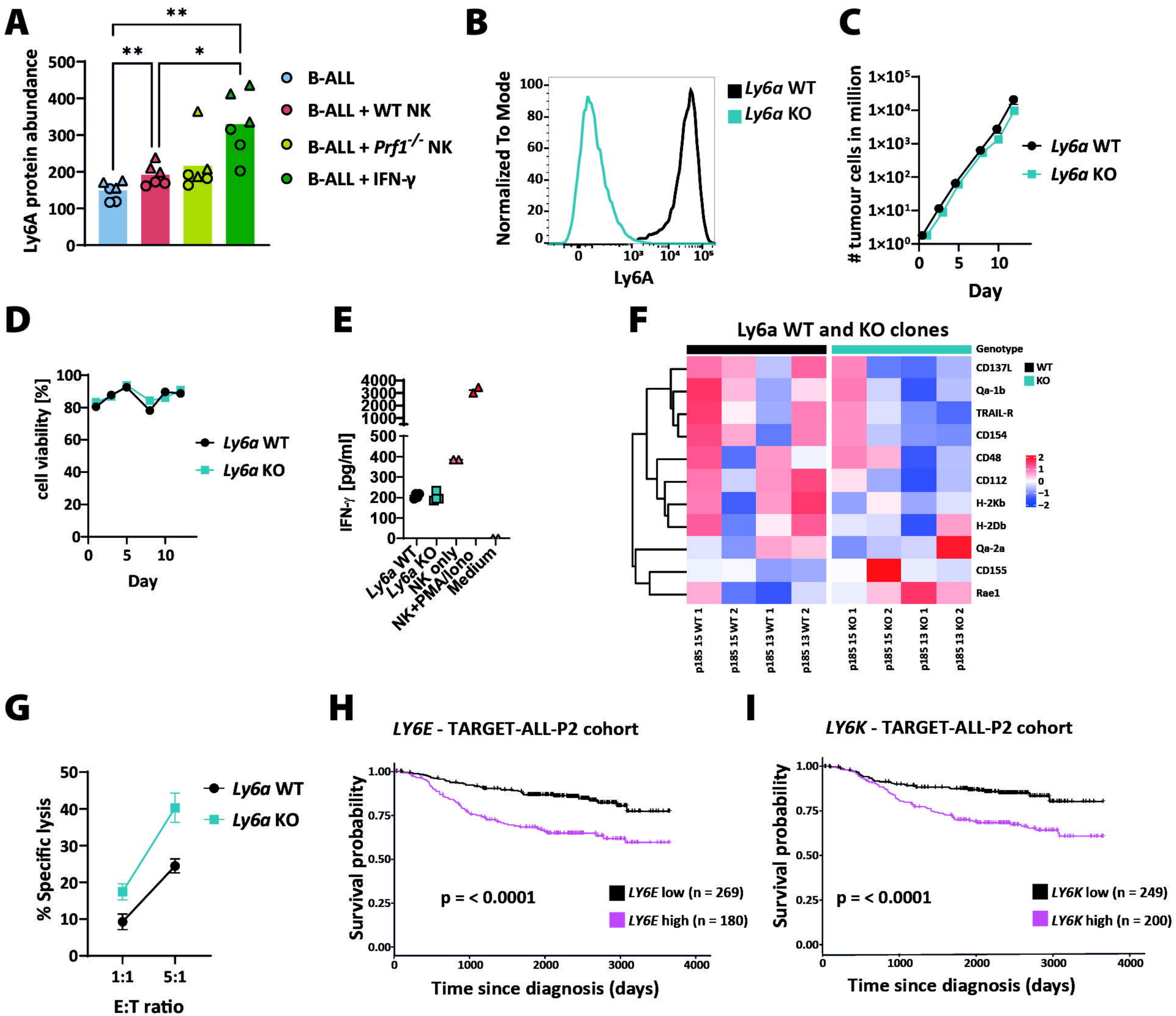
A
Ly6A protein abundance
B-ALL
B-ALL + WT NK
B-ALL + Prf1-/- NK
B-ALL + IFN-γ
B
Normalized To Mode
Ly6A
Ly6a WT
Ly6a KO
C
tumour cells in million
Day
Ly6a WT
Ly6a KO
D
cell viability [%]
Day
Ly6a WT
Ly6a KO
E
IFN-γ [pg/ml]
Ly6a WT
Ly6a KO
NK only
NK+PMA/Iono
Medium
F
Ly6a WT and KO clones
Genotype
WT
KO
CD137L
Qa-1b
TRAIL-R
CD154
CD48
CD112
H-2Kb
H-2Db
Qa-2a
CD155
Rae1
p185 15 WT 1
p185 15 WT 2
p185 13 WT 1
p185 13 WT 2
p185 15 KO 1
p185 15 KO 2
p185 13 KO 1
p185 13 KO 2
G
% Specific lysis
E:T ratio
Ly6a WT
Ly6a KO
H
LY6E - TARGET-ALL-P2 cohort
Survival probability
p = < 0.0001
LY6E low (n = 269)
LY6E high (n = 180)
Time since diagnosis (days)
I
LY6K - TARGET-ALL-P2 cohort
Survival probability
p = < 0.0001
LY6K low (n = 249)
LY6K high (n = 200)
Time since diagnosis (days)